

A Survey on 3D-aware Image Synthesis

Weihao Xia and Jing-Hao Xue, *Senior Member, IEEE*

Abstract—Recent years have seen remarkable progress in deep learning powered visual content creation. This includes 3D-aware generative image synthesis, which produces high-fidelity images in a 3D-consistent manner while simultaneously capturing compact surfaces of objects from pure image collections without the need for any 3D supervision, thus bridging the gap between 2D imagery and 3D reality. The 3D-aware generative models have shown that the introduction of 3D information can lead to more controllable image generation. The task of 3D-aware image synthesis has taken the field of computer vision by storm, with hundreds of papers accepted to top-tier journals and conferences in recent year (mainly the past two years), but there lacks a comprehensive survey of this remarkable and swift progress. Our survey aims to introduce new researchers to this topic, provide a useful reference for related works, and stimulate future research directions through our discussion section. Apart from the presented papers, we aim to constantly update the latest relevant papers along with corresponding implementations at <https://weihaox.github.io/awesome-3D-aware-synthesis>.

Index Terms—Deep learning, computer vision, generative models, implicit neural representation, novel view synthesis

1 INTRODUCTION

A tremendous amount of progress has been made in deep generative models that lead to photorealistic image synthesis. Despite achieving compelling results, most approaches focus on two-dimensional (2D) images, overlooking the three-dimensional (3D) nature of the physical world. The lack of 3D structure, therefore, inevitably limits some of their practical applications. Several recent works therefore propose generative models that are 3D-aware, *i.e.*, scenes are modeled in 3D and then rendered differentially to the image plane. In contrast to the 2D generative models, the recently developed 3D-aware generative models [1], [2] bridge the gap between 2D images and 3D physical world. The physical world surrounding us is intrinsically three-dimensional and images depict reality under certain conditions of geometry, material, and illumination, making it natural to model the image generation process in 3D spaces. As shown in Fig. 1, classical rendering (a) renders images at certain camera positions given human-designed or scanned 3D shape models; inverse rendering (b) recovers the underlying intrinsic properties of the 3D physical world from 2D images; 2D image generation (c) is mostly driven by generative models, which have achieved impressive results in photorealistic image synthesis; and 3D-aware image synthesis (d) offers the possibility of replacing the classical rendering pipeline with effective and efficient models that are learned directly from images.

Despite striking progress has been made recently in research of 3D-aware image synthesis, it lacks a timely and systematic review of this progress. In this work, we fill the gap by presenting a comprehensive survey of the latest research in 3D-aware image synthesis methods. We envision that our work will elucidate design considerations and advanced methods for 3D-aware image synthesis, present its advantages and disadvantages of different kinds, and suggest future research directions. We provide an outline and taxonomy of this survey in Fig. 2. We propose to categorize

the 3D-aware image synthesis methods into three categories: 3D control of 2D generative models (§ 3), 3D novel view synthesis from multiple views (§ 4), and 3D generative models from single views (§ 5). Then, every category is further divided into some subcategories depending on the experimental setting or the specific utilization of 3D information. In particular, 3D control of 2D generative models are further divided into 1) 3D control latent directions (§ 3.1), 2) 3D parameters as controls (§ 3.2), and 3) 3D priors as constraints (§ 3.3). Both § 4 and § 5 summarize methods that target generating photorealistic and multi-view-consistent images by learning 3D representations. Broadly speaking, both categories leverage neural 3D representations to represent scenes, use differentiable neural renderers to render them into the image plane, and optimize the network parameters by minimizing the difference between rendered images and observed images. However, they are significantly different in training on a multiple-view or single-view image collections, due to their hugely different application scenarios. Moreover, in order to present these representative generative 3D-aware image synthesis methods intuitively, we show a chronological overview in Fig. 3 by organizing them into the three aforementioned paradigms.

Here, we present a timely up-to-date overview of the growing field of 3D-aware image synthesis. Considering the lack of a comprehensive survey and an increasing interest and popularity, we believe it necessary to organize one to help computer vision practitioners with this emerging topic. The purpose of this survey is to provide researchers new to the field with a comprehensive understanding of 3D-aware image synthesis methods and show the superior performance over the status quo approaches. To conclude, we highlight several open research directions and problems that need further investigation. The scope of this fast-expanding field is rather extensive and a panoramic review would be challenging. We shall present only representative methods of 3D-aware image synthesis rather than listing exhaustively all literature. This review can therefore serve as a pedagogical tool, providing researchers with the key information about typical methods of 3D-aware image synthesis.

- W. Xia and J.-H. Xue are with the Department of Statistical Science, University College London, London, UK.
E-mail: xiawh3@outlook.com, jinghao.xue@ucl.ac.uk

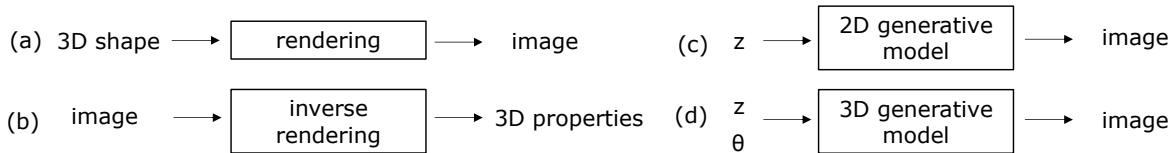


Fig. 1. Comparison of (a) rendering, (b) inverse rendering, (c) 2D generative models and (d) 3D generative models. 3D generative models learn 3D representations first and then render a 2D image at certain viewpoints. Both 2D and 3D generative models have unconditional and conditional settings. An unconditional generative model maps a noise input z (and a camera pose in 3D models) to a fake image; a conditional model takes an additional input as the control signal, which could be another image, text, or a categorical label.

Researchers can use these general guidelines to develop the most appropriate technique for their own particular study. The main technical contributions of this work are as follows:

- Hierarchical taxonomy. We propose a systematic taxonomy for 3D-aware image synthesis research. We categorize existing models into three categories: 3D control of 2D generative models, 3D generative models from single views, and novel view synthesis from multiple views.
- Comprehensive review. We provide a comprehensive overview of the existing state-of-the-art 3D-aware image synthesis methods. We compare and analyze the main characteristics and improvements for each type, assessing their strengths and weaknesses.
- Outstanding challenges. We present open research problems and provide some suggestions for the future development of 3D-aware image synthesis.
- In an attempt to continuously track recent developments in this fast advancing field, we provide an accompanying webpage which catalogs papers addressing 3D-aware image synthesis, according to our problem-based taxonomy: <https://weihaox.github.io/awesome-3D-aware-synthesis>.

2 BACKGROUND

This section introduces a few important concepts as the background. In order to formulate 3D-aware image synthesis, we first clarify how 2D and 3D data are expressed, and how they are converted between each other. Moreover, we introduce two key elements involved in most 3D-aware image synthesis methods: implicit neural representations and differentiable neural rendering.

2.1 2D and 3D Data, Rendering and Inverse Rendering

The 2D images depict a glimpse into the surrounding 3D physical world with its geometry, materials, and illumination conditions at that moment. Images are composed of an array of pixels (picture elements). The 3D reality can be represented in many different ways, each with its own advantages and disadvantages. There are several examples of such **3D shape representations**, including depth images, point clouds, voxel grids, and meshes. **Depth images** contain distance information between the object and the camera at every pixel. The distance encodes 3D geometry information from a fixed point of view. Layered depth images (LDIs) use several layers of depth maps and their associated color values to depict a scene. **Point clouds** comprise vertices in 3D space, represented by coordinates along the x , y , and z axes. These types of data can be

acquired by 3D scanners, such as LiDARs or RGB-D sensors, from one or more viewpoints. **Voxel grids** describe a scene or object using a regular grid in 3D space. A voxel (volume element) in 3D space is analogous to a pixel in a 2D image. A voxel grid can be created from a point cloud by voxelization, which groups all 3D points within a voxel. **Meshes** are a collection of vertices, edges, and polygonal faces. In contrast to a point cloud, which only provides vertices locations, a mesh also provides surface information of an object. Nevertheless, deep learning does not provide a straightforward way to process surface information. Instead, many techniques resort to sampling points from the surfaces to create a point cloud from the mesh representation.

As shown in Fig. 1(a), images can be obtained by rendering a 3D object or scene under certain viewpoints and lighting conditions. This forward process is called **rendering** (image synthesis). Rendering has been studied in computer graphics and a wide variety of renderers are available for use. The reverse process, **inverse rendering**, as shown in Fig. 1(b), is to infer underlying intrinsic components of a scene from rendered 2D images. These properties include shape (surface, depth, normal), material (albedo, reflectivity, shininess), and lighting (direction, intensity), which can be further used to render photorealistic images. The inverse rendering papers are not classified as 3D-aware image synthesis methods in this survey as they are not deliberately designed for this purpose. 3D-aware image synthesis in this survey include a similar inverse rendering process and a rendering process. In contrast, these methods typically do not produce explicit 3D representations such as meshes or voxels for rendering. They learn **neural 3D representations** (mostly implicit functions), render them into images with **differentiable neural rendering** technique, and optimize the network parameters by minimizing the difference between the observed and rendered images.

2.2 Implicit Scene Representations

In computer vision and computer graphics, 3D shapes are traditionally represented as explicit representations like depths, voxels, point clouds, or meshes. Recent methods propose to represent 3D scenes with neural implicit functions, such as occupancy field [3], signed distance field [4], and radiance field [5]. The implicit neural representation (INR, neural fields, or coordinate-based representation) is a novel way to parameterize signals across a wide range of domains. Taking images as an example, INR parameterizes an image as a continuous function that maps pixel coordinates to RGB colors. The implicit functions are often not analytically tractable and are hence approximated by neural networks. Here are some popular examples of INR.

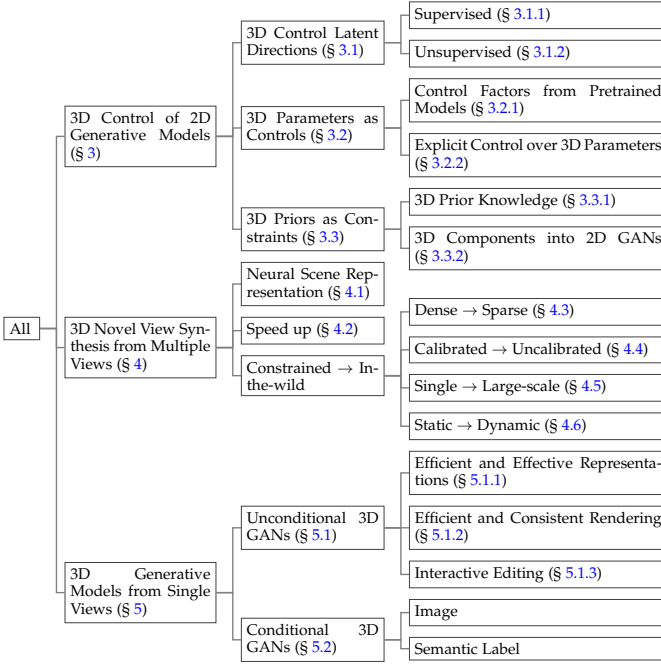


Fig. 2. A systematic taxonomy proposed in this survey of 3D-aware image synthesis methods.

Occupancy Field [3], [6], [7] implicitly represents a 3D surface with the continuous decision boundary of a neural classifier. This function approximated with a neural network assigns to every location $p \in \mathbb{R}^3$ an occupancy probability between 0 and 1. Given an observation (e.g., image or point cloud) $x \in \mathcal{X}$ and a location $p \in \mathbb{R}^3$, the representation can be simply parameterized by a neural network f_θ that takes a pair (p, x) as input and outputs a real number which represents the probability of occupancy: $f_\theta : \mathbb{R}^3 \times \mathcal{X} \rightarrow [0, 1]$.

Signed Distance Field [4] is a continuous function that models the distance from a queried location to the nearest point on a shape’s surface, whose sign indicates if this location is inside (negative) or outside (positive): $SDF(\mathbf{x}) = s, \mathbf{x} \in \mathbb{R}^3, s \in \mathbb{R}$. The underlying surface is implicitly described as the zero iso-surface decision boundaries of feed-forward networks $SDF(\cdot) = 0$. This implicit surface can be rendered by raycasting or rasterizing a mesh obtained through marching cubes [8].

Radiance Field [5] (NeRF) has attracted growing attention due to its compelling results in novel view synthesis on complex scenes. It leverages an MLP network to approximate the radiance fields of static 3D scenes and uses the classic volume rendering technique [9] to estimate the color of each pixel. This function takes as input a 3D location \mathbf{x} and 2D viewing direction \mathbf{d} , and outputs a directional emitted RGB color c and volume density σ : $f_\theta : (\mathbf{x}, \mathbf{d}) \rightarrow (c, \sigma)$. It captures 3D geometric details based on pure 2D supervision by learning the reconstruction of given views.

There also exist many other implicit functions proposed to represent a scene, such as neural sparse voxel fields [10], or neural volumes [11].

2.3 Differentiable Neural Rendering

3D rendering is a function that outputs a 2D image from a 3D scene. Differentiable rendering provides a differentiable

rendering function, that is, it computes the derivatives of that function in response to different parameters of the scene. Once a renderer is differentiable, it can be integrated into the optimization of neural networks. One use case for differentiable rendering is to compute a loss in rendered image space and back propagation can be applied to train the network. Driven by the prevalence of NeRF-based methods [5], volume rendering [9] becomes the most commonly used differentiable renderer among the methods that this survey targets. It is naturally differentiable, and the only input required to optimize the NeRF representation is a set of images with known camera poses. In [5], given volume density and color functions, volume rendering is used to obtain the color $C(\mathbf{r})$ of any camera ray $\mathbf{r}(t) = \mathbf{o} + t\mathbf{d}$, with camera position \mathbf{o} and viewing direction \mathbf{d} using

$$C(\mathbf{r}) = \int_{t_1}^{t_2} T(t) \cdot \sigma(\mathbf{r}(t)) \cdot c(\mathbf{r}(t), \mathbf{d}) \cdot dt, \quad (1)$$

where

$$T(t) = \exp\left(-\int_{t_1}^t \sigma(\mathbf{r}(s)) ds\right). \quad (2)$$

$T(t)$ denotes the accumulated transmittance, representing the probability that the ray travels from t_1 to t without being intercepted. The rendered image can be obtained by tracing the camera rays $C(\mathbf{r})$ through each pixel of the to-be-synthesized image.

2.4 Dataset

Based on the experimental setting and applicable scenarios, different categories of target papers use either multiple views or single views of the image collections. Multiple-view image datasets contain images of a scene taken from different viewpoints and are usually used in novel view synthesis (see § 4). Similar to 2D models, 3D-aware generative models (see § 5) aim to produce photorealistic and multi-view consistent images. Therefore, the same single-view image datasets are used as in the 2D methods.

2.4.1 Multiple-view image collections

Per-scene multiple-view image collections are usually used in the novel view synthesis methods. These methods aim to learn effective and expressive 3D representations and render novel view images or produce free-viewpoint videos from a collection of multiple-view images. Tab. 1 shows some example of multi-view image datasets. In early studies, input data must meet several strong assumptions, including diverse camera views, precise intrinsic and extrinsic camera parameters, and constant lighting conditions. Therefore, most of them either use synthetic data rendered from 3D scans or real images captured from real world, along with corresponding camera parameters and scene bounds. For synthetic data, they use ground-truth camera poses, intrinsics, and bounds; for real data, they use the off-the-shelf softwares (e.g. a structure-from-motion package COLMAP [65]) to estimate these parameters. Typically, it requires sufficient camera diversity and coverage over repeated observations of a target object or scene. An example of synthetic data rendering process is to center a scan (e.g., objects from ScanNet [66], ShapeNet [67], or DeepVoxels [14]) at the origin, scale it to lie within the unit cube, and render images at sampled viewpoints. The training set can be obtained by

TABLE 1
Examples of multi-view image datasets.

dataset	published in	# scene	# samples per scene	range (m ²)	resolution	used in	keyword
DeepVoxels [14]	CVPR 2019	4 simple objects	479 / 1,000	\	512 × 512	[5]	synthetic, 360 degree
NeRF Synthetics [5]	ECCV 2020	8 complex objects	100 / 200	\	800 × 800	[5], [37]	synthetic, 360 degree
NeRF Captured [5]	ECCV 2020	8 complex scenes	20-62	a few	1,008 × 756	[5]	real, forward-facing
DTU [68]	CVPR 2014	124 scenes	49 or 64	a few to thousand	1,600 × 1,200	[70], [71]	often used in few-views
Tanks & Temples [72]	CVPR 2015	14 objects and scenes	4,395 - 21,871	dozen to thousand	8-megapixel	[73]	real, large-scale
Phototourism [74]	IJCV 2021	6 landmarks	763-2,000	dozen to thousand	564-1,417 megapixel	[75]	varying illumination
Alamo Square [53]	CVPR 2022	San Francisco	2,818,745	570 × 960	1,200 × 900	[53]	real, large-scale

3D metrics access the shape and surface quality, as well as the temporal and multi-view consistency. Model efficiency is taken into account sometimes and is evaluated by model size and training/inference time.

2.5.1 Model Efficiency

Current methods use two metrics to show the efficiency of their proposed methods: average running time and model complexity. Such metrics can be borrowed from deep compression, which evaluates inference runtime, model size and latency. The model complexity is typically assessed by the number of parameters, floating point operations (FLOPs), and multiply-accumulate operations (MACs). Runtime usually means one forward at inference phase. In our case, inference runtime means the time required for rendering an image. But for 3D image synthesis, we also care about the time required for training, which could be evaluated by total training time and batches per second [44].

2.5.2 Image Quality and Diversity

These metrics are often used to assess images generated by a generative model, like a generative adversarial network (GAN), mostly in § 3.2 and § 5. These metrics include but are not limited to Inception Score (IS) [84], Fréchet Inception Distance (FID) [85], and Learned Perceptual Image Patch Similarity (LPIPS) [86].

IS is to measure the quality and diversity of images generated from GAN models. It calculates the statistics of a synthesized image using Inception-v3 Network [87] pretrained on ImageNet [88]. A higher score is better.

FID is defined by the Fréchet distance between features from the real and generated images based on Inception-v3 [87]. Lower FID indicates better perceptual quality.

KID measures the dissimilarity between two probability distributions using samples drawn independently from each distribution. Lower is better.

LPIPS measures image perceptual quality using a VGG model [89] pretrained on ImageNet. A lower value means higher similarity between image patches.

2.5.3 Image Fidelity

Fidelity (or faithfulness) measures the similarity between real images and generated ones. The most widely used metrics are Peak Signal-to-Noise Ratio (PSNR) and Structural Similarity (SSIM) [90]. The pixel-wise reconstruction distances, *e.g.* mean absolute error, are also used.

PSNR between the ground-truth image and the reconstruction is defined by the maximum possible pixel value of the image and the mean squared error between images.

SSIM measures the structural similarity between images based on independent comparisons in terms of luminance, contrast, and structures. The details can be found in [90].

2.5.4 Multi-view 3D Consistency

Multi-view 3D consistency is another significantly important aspect in 3D-aware image synthesis. The view-inconsistencies could be caused by shapes and colors. The consistency in photometry and geometry is basically equivalent to the quality of shape and texture.

Shape Quality is evaluated mostly by calculating differences between the rendered depth map and the pseudo-ground-truth depth, *e.g.* using MSE [48] or a modified Chamfer distance [50]. For example, given two generated images from two sampled angles of the same scene, Shi *et al.* [52] uses rotation precision and rotation consistency to evaluate the quality of the depth maps (point cloud). The former is aimed to measure the accuracy of the angle of rotation while the latter targets at the rotation consistency evaluation. In GOF [45], the mean angle deviation (MAD) and the scale-invariant depth error (SIDE) are used to compare the outputs against the ground-truth depth maps. MAD emphasizes the compactness of surfaces, whereas SIDE emphasizes the accuracy of depths. Some methods use more direct indicators to evaluate the geometry properties of learned surfaces. Xu *et al.* [45] use average geodesic distance and average curvature between random points to assess the geometry properties of learned surfaces. The lower these two metrics, the smoother the recovered object surfaces.

Texture Quality could be evaluated by using PSNR and SSIM as image fidelity under different viewpoints. But in most cases, the ground-truth images are not available for evaluation. Several methods use FID to evaluate image quality at different camera poses as part of the multi-view texture quality. A more direct way is to assess multi-view facial identity consistency (ID) [48] by calculating the mean Arcface [91] cosine similarity score between pairs of the same face rendered from random camera poses.

Apart from the aforementioned performance measures, pose accuracy [48] is also considered as an important indicator of shape quality and controllability. Poses (pitch, yaw, and roll) are detected with the help of pre-trained face reconstruction models from the generated images and then its L2 errors against the ground-truth poses is computed to determine each model’s pose drift.

In the following sections, we introduce different kinds of 3D-aware image synthesis methods. The first (arXiv) draft dates are used to sequence the publications. The publication information can be found in the bibliography. Tab. 3 is a detailed comparison of 3D-aware image synthesis methods.

3 3D CONTROL OF 2D GENERATIVE MODELS

Due to the prevalence of 2D generative models, there have been studies aiming to make these pretrained models, especially GANs, 3D aware. These works, mostly built on the

TABLE 2

Summary of popular single-view image datasets organized by their major categories and roughly sorted by their popularity.

dataset	published in	category	# samples	resolution	representative references	keyword
FFHQ [78]	CVPR 2019	Human Face	70k	1024 × 1024	[1], [48], [50], [51]	single simple-shape
AFHQ [82]	CVPR 2020	Cat, Dog, and Wildlife	15k	512 × 512	[1], [48], [50], [51]	single simple-shape
CompCars [72]	CVPR 2015	Real Car	136K	256 × 256	[1], [16], [20], [51]	single simple-shape
CARLA [79]	CoRL 2017	Synthetic Car	10k	128 × 128	[2], [49], [51], [58], [71]	single simple-shape
CLEVR _m [81]	CVPR 2017	Objects	100k	256 × 256	[20], [32]	multiple, simple-shape
LSUN [80]	2015	Bedroom	300K	256 × 256	[16], [51]	single, simple-shape
CelebA [76]	ICCV 2015	Human Face	200k	178 × 218	[16], [51]	single simple-shape
CelebA-HQ [77]	ICLR 2018	Human Face	30k	1024 × 1024	[46]	single, simple-shape
MetFaces [83]	NeurIPS 2020	Art Face	1336	1024 × 1024	[1]	single, simple-shape
M-Plants [60]	NeurIPS 2022	Variable-Shape	141,824	256 × 256	[60]	single, variable-shape
M-Food [60]	NeurIPS 2022	Variable-Shape	25,472	256 × 256	[60]	single, variable-shape

top of a pretrained StyleGAN, can be further categorized into three groups based on how the 3D control capability is introduced: 1) discovering 3D control latent directions, 2) adopting explicit control over the 3D parameters, and 3) introducing 3D-aware components into 2D GANs. Fig. 4 is an illustration of these three categories of methods.

3.1 Discovering 3D Control Latent Directions

It has been demonstrated that pretrained GANs have interpretable directions in their latent spaces. The image generation process is controlled by altering the latent codes \mathbf{z} in the desired directions \mathbf{n} with step α , which is often considered as a linear vector arithmetic $\mathbf{z}' = \mathbf{z} + \alpha\mathbf{n}$. The altered latent codes are then fed into a pretrained GAN $G(\cdot)$ for the edited results: $I' = G(\mathbf{z}')$. The methods in this group are mostly developed for semantic editing, and some have been shown to discover geometric directions as well. They are used to alter pose position or light condition of faces or manipulate geometry (e.g. zoom, shift, or rotation) of natural images. As classified in [96], such directions can be identified through supervised, self-supervised, or unsupervised manners.

3.1.1 Supervised Manner

These methods typically sample a large amount of latent codes, synthesize a collection of corresponding images, and annotate them with predefined labels by introducing a pretrained classifier. For example, to interpret the face representation learned by GANs, Shen *et al.* [25] (May 2020) employ some off-the-shelf classifiers to learn a hyperplane in the latent space serving as the separation boundary and predict semantic scores for synthesized images. Even though the boundary is searched by solving a bi-classification problem, it can produce continuous face pose changing by moving the latent code. Abdal *et al.* [97] (Aug 2020) learn a bidirectional mapping between the \mathcal{Z} space and the \mathcal{W} space by using continuous normalizing flows (CNF). Attribute information (including head poses) are injected into the CNF blocks for the desired results. However, such methods rely on the availability of attributes (typically obtained by a face classifier network), which might be difficult to obtain for new datasets and could require manual labeling effort. Jahanian *et al.* [18] (Jul 2019) use a self-supervised manner to learn these directions without any direct supervision. Sequence of target images are obtained by applying simple augmentations to the source image. Specifically, image shifting is used for camera motion along vertical and horizontal axes, downsampling and central cropping for zooming in and out, and perspective transformation for rotation. With

inverted images $G(\mathbf{z})$ and target edits $\text{edit}(G(\mathbf{z}), \alpha)$, they learn the direction \mathbf{n} by minimizing the distance between the generated image $G(\mathbf{z} + \alpha\mathbf{n})$ after taking an α -step in the latent direction and the target image $\text{edit}(G(\mathbf{z}), \alpha)$.

3.1.2 Unsupervised Manner

Some methods [21], [24] aim to discover interpretable directions in the latent space in an unsupervised manner, *i.e.*, without the requirement of paired data. For example, Härkönen *et al.* [24] (Apr 2020) create interpretable controls for image synthesis by identifying important latent directions based on PCA applied in the latent or feature space. The obtained principal components correspond to certain attributes, and the selective application of the principal components allows for the control of many image attributes. Some of their discovered directions support 3D operations such as rotation or zooming out. This method is considered as “unsupervised” since the directions can be discovered by PCA without using any labels. There is still a need to manually annotate these directions to the target operations and to which layers they should be applied to.

In [27], Shen *et al.* (Jul 2020) show that latent directions for 3D-aware image synthesis can be directly computed in a closed form without any kind of training or optimization. They propose a **Semantics Factorization** (SeFa) method based on the singular value decomposition of the weights of the first layer of a pretrained GAN. They observe that the semantic transformation of an image, usually denoted by moving the latent code toward a certain direction $\mathbf{n}' = \mathbf{z} + \alpha\mathbf{n}$, is only determined by the latent direction \mathbf{n} . Therefore, the directions \mathbf{n} can cause a significant change in the output image $\Delta\mathbf{y}$, *i.e.*, $\Delta\mathbf{y} = \mathbf{y}' - \mathbf{y} = (\mathbf{A}(\mathbf{z} + \alpha\mathbf{n}) + \mathbf{b}) - (\mathbf{A}\mathbf{z} + \mathbf{b}) = \alpha\mathbf{A}\mathbf{n}$, where \mathbf{A} and \mathbf{b} are respectively the weight and bias of certain layers in G . The obtained formula, $\Delta\mathbf{y} = \alpha\mathbf{A}\mathbf{n}$, suggests that the desired editing with direction \mathbf{n} can be achieved by adding the term $\alpha\mathbf{A}\mathbf{n}$ onto the projected code and indicates that the weight parameter \mathbf{A} should contain the essential knowledge of image variations. The eigenvectors of the matrix $\mathbf{A}^T\mathbf{A}$ should be the desired directions \mathbf{n}^* . This gives a closed-form factorization of latent semantics in GANs. This method supports multiple 3D control operations such as car orientation, face and body pose, streetscape and bedroom viewpoint, zoom, shift, as well as rotation on a variety of GANs.

3.2 Incorporating 3D Parameters as Controls

Methods using 3D parameters as control factors typically follow a paradigm described as $x' = G(x, \theta)$. Explicit

TABLE 3

Overview of 3D-controllable image generation. *Condition* means the input besides noise vectors, such as images, 3D control parameters, or viewpoints. The term *location* and *view* represent the 3D location (world coordinate) $x = (x, y, z)$ and the 2D viewing direction (θ, ϕ) . *Dataset* means what kinds of images these methods used for training. Those trained on single-view imagery usually only supports a single image *Category*. For multiple-view imagery, these images can be densely or sparsely sampled (captured) multiple views of a scene, bounded or unbounded, static or dynamic. *Posed images* mean 2D images along with their respective extrinsic and intrinsic camera matrices. *Geometry* indicates if the model is available for geometry reconstruction. *Editability* means if the model has the ability of attribute edit beyond camera pose.

Method	Publication	Dataset / Category	Condition	Geometry	Editability	Supervision	Highlight
3D Latent Control Directions							
GANSteerability [18]	ICLR 2020	ImageNet	N/A	✗	✓	shifted image	
GANLatentDiscovery [21]	ICML 2020	face, ILSVRC	N/A	✗	✓	unsupervised	
InterFaceGAN [25]	CVPR 2020	face	N/A	✗	✓	synthetic image & label	
GANSpace [24]	NeurIPS 2020	face, ImageNet	N/A	✗	✓	unsupervised	
SeFa [27]	CVPR 2021	face, car, LSUN, ImageNet	N/A	✗	✓	closed-form	
3D Parameters as Controls							
StyleRig [22]	CVPR 2020	face	GAN-generated image	✗	✓	3DMM	
DiscoFaceGAN [55]	CVPR 2020	face	parameters	✗	✓	3DMM	
PIE [30]	TOG 2020	face	real image	✗	✓	3DMM	
CONFIG [23]	ECCV 2020	face	real image / parameters	✗	✓	synthetic data	
GAN-Control [34]	ICCV 2021	face	parameters	✗	✓	pseudo param.	
3D-FM GAN [64]	ECCV 2022	face	real image and rendering	✗	✓	synthetic data	
3D Priors as Constraints							
S^2 -GAN [12]	ECCV 2016	scene (NYUv2)	unconditional	✗	✗	normal map	
PrGANs [13]	3DV 2017	synthesized from 3D shapes	unconditional	✓	✗	image and viewpoint	
VON [15]	NeurIPS 2018	chair, car	unconditional	✓	✗	2.5D sketch, 3D shape	
RGBD-GAN [19]	ICLR 2020	face, car	camera parameters	✓(depth)	✗	unsupervised	
NGP [26]	CGF 2021	chair, car	user controls	✓	✓	3D shape, reflectance map	
LiftedGAN [92]	CVPR 2021	face	unconditional	✓	✓	pseudo multi-view images	
DepthGAN [52]	ECCV 2022	scene (LSUN)	viewpoint	✓(depth)	✓	pseudo depth map	
3D Novel View Synthesis (from multi-view imagery)							
DeepVoxels [14]	CVPR 2019	dense bounded static scene	view, image	✗	✗	multi-view posed images	
SRN [17]	NeurIPS 2019	dense bounded static scene	view, location	✓	✓	multi-view posed images	
DVR [7]	CVPR 2020	dense bounded static scene	view, location	✓	✗	multi-view posed images	
NeRF [5]	ECCV 2020	dense bounded static scene	view, location	✗	✗	multi-view posed images	
NeRF++ [31]	2020	dense unbounded static scene	view, location	✗	✗	multi-view posed images	
NeRF-W [29]	CVPR 2021	dense bounded static scene	view, location	✗	✗	unconstrained posed images	
PixelNeRF [33]	CVPR 2021	sparse bounded static scene	view, location	✗	✗	one or a few posed images	
FastNeRF [38]	CVPR 2021	dense bounded static scene	view, location	✗	✗	multi-view posed images	
KiloNeRF [36]	CVPR 2021	dense bounded static scene	view, location	✗	✗	multi-view posed images	
D-NeRF [93]	CVPR 2021	dynamic scene	view, location	✗	✗	multi-view posed images	
BARF [40]	ICCV 2021	dense bounded static scene	view, location	✗	✗	multi-view unposed images	
NeRF— [35]	2021	dense front-facing static scene	view, location	✗	✗	unposed front-facing images	
LFN [94]	NeurIPS 2022	dense bounded static scene	image, pose	✗	✗	multi-view posed images	light field
Block-NeRF [53]	CVPR 2022	large-scale scene	view, location	✗	✗	unconstrained posed images	
Instant-NGP [54]	TOG 2022	dense bounded static scene	view, location	✗	✗	multi-view posed images	
3DiM [95]	2022	dense bounded static scene	image, pose	✗	✗	posed images	diffusion model
3D Generative Models (from single-view imagery)							
HoloGAN [16]	ICCV 2019	face, cat, car, LSUN	camera pose	✗	✗	unsupervised	deep voxel
Liao <i>et al.</i> [42]	CVPR 2020	multiple object data	unconditional	✓	✗	unsupervised	3D primitives
BlockGAN [20]	NeurIPS 2020	multiple object data	camera pose	✗	✓	unsupervised	deep voxel
GRAF [28]	NeurIPS 2020	rendered chair, face, cat, bird	camera matrix, pose	✗	✗	unsupervised	NeRF
pi-GAN [2]	CVPR 2021	face, car, CARLA	camera position	✓	✗	unsupervised	NeRF
GIRAFFE [32]	CVPR 2021	chair, cat, face, car, church	camera pose	✗	✓	unsupervised	compositional NeRF
GOF [45]	NeurIPS 2021	cat, car, face	3D location, camera pose	✓	✗	unsupervised	generative occupancy fields
ShadeGAN [43]	NeurIPS 2021	cat, face	3D location, camera pose	✓	✗	unsupervised	light field
CAMPARI [59]	3DV 2021	cat, car, face, chair	camera pose	✗	✓	unsupervised	decomposed NeRF
StyleNeRF [1]	ICLR 2022	face, cat, car	camera pose	✓	✗	unsupervised	NeRF
GRAM [49]	CVPR 2022	cat, face, CARLA	camera pose	✗	✗	unsupervised	
EG3D [48]	CVPR 2022	cat, face	camera parameters	✓	✗	unsupervised	tri-plane 3D representation
VolumeGAN [51]	CVPR 2022	cat, car, face, bedroom, CARLA	camera pose	✓	✗	unsupervised	
StyleSDF [50]	CVPR 2022	cat, face	camera pose	✓	✗	unsupervised	SDF
Pix2NeRF [71]	CVPR 2022	face, CARLA, rendered image	image	✗	✗	unsupervised	
Sem2NeRF [57]	ECCV 2022	cat, face	semantic mask, camera pose	✗	✗	semantic mask and image	
SURF-GAN [63]	ECCV 2022	face	camera pose	✗	✗	unsupervised	
EpiGRAF [60]	NeurIPS 2022	cat, face, variable-shape	camera pose	✓	✗	unsupervised	tri-plane 3D representation
IDE-3D [61]	TOG 2022	face	camera pose	✓	✓	semantic mask and image	tri-plane 3D representation

control over the 3D parameters θ gives the edited result x' . Here, θ could be human-interpretable attribute descriptions or a set of parameters from 3D models. Sometimes, the given control factors are intuitively understandable, *e.g.*, (age: 20 years old), (head pose: pitch, yaw, roll), or using the environment map to represent light condition. Most methods in this category incorporate 3D pretrained model parameters into 2D image-based generative models for controllable 3D-aware synthesis. These methods propose solutions to translate controls of 3D face rendering models into GAN-generated processes. Taking face generation as an example, they usually integrate priors from a parametric 3D Morphable Model (3DMM) [98] as explicit control factors. Tab. 4 is an overview of methods that incorporate 3D parameters to a 2D generative model.

The models in this section, as well as those in the next, make use of additional 3D models. Their main difference is

that the former uses 3D model parameters as input control factors while the latter uses them as supervision signals. There is another series of studies combining implicit 3D representation with 3DMM, either being trained with a reconstruction loss using annotated multi-view datasets [99] or directly imposing 3DMM conditions into 3D NeRF volume and being trained on unannotated single-view images [100]. We focus on leveraging 3D priors for image synthesis based on 2D generative models and will introduce other studies in the remaining sections.

3.2.1 Control Factors from Pretrained Models

Most methods use 3DMM parameters to provide explicit control. 3DMMs is commonly used to represent faces, where faces are parameterized by head rotation ϕ and translation ρ , identity geometry α , expressions β , skin reflectance δ , and scene illumination γ : $\theta = (\phi, \rho, \alpha, \delta, \beta, \gamma) \in \mathbb{R}^m$. The parametric nature of 3DMMs allows navigating and explor-

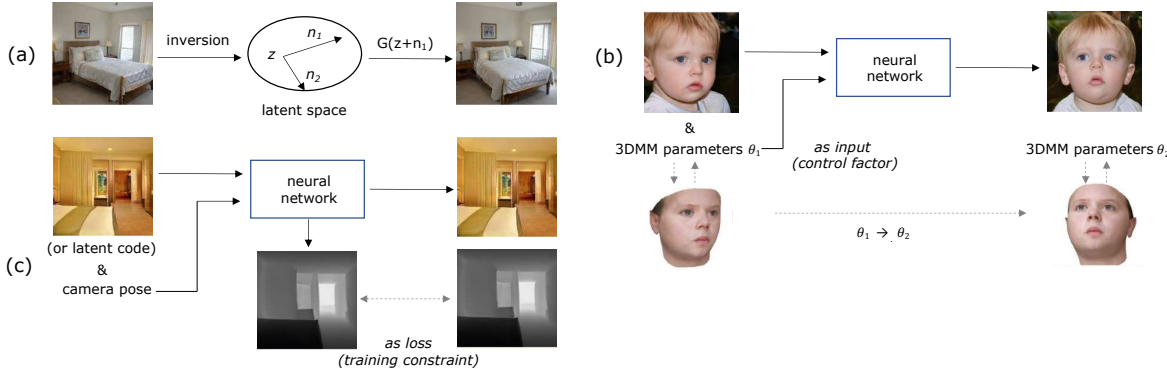


Fig. 4. Comparison of methods aiming to make 2D generative models (mostly GANs) 3D aware. These works are categorized into three groups based on how the 3D control capability is introduced: a) discovering 3D control latent directions in the pretrained GAN latent spaces, b) using 3D parameters (e.g. from 3DMM [98]) as input for explicit control, and c) introducing 3D-aware components (e.g. depth estimation module) into 2D GANs and adopting 3D prior knowledge (e.g. depth map) as training constraints.

ing the space of plausible faces. Thus, synthetic images can be rendered based on different parameter configurations. In practice, these 3DMM parameters are first transformed before being used in the network [30], [55]. Besides 3DMM, parameters from other state-of-the-art tools could also be used to provide 3D control factors. In [97], Microsoft Face API predicts pitch and yaw as the head pose. GAN-Control [34] extracts head-pose, expression, illumination, age, and hair color by using several off-the-shelf attribute predictors. DiscoFaceGAN [55] extracts identity, expression, and texture information from 3DMM, approximates scene illumination with Spherical Harmonics (SH) [101], and defines face pose as three rotation angles.

For this category, a key question is how to associate these parameters with corresponding images as these methods require supervised training. Except one using existing synthetic data with 3D parameters [23], others use pretrained models to achieve transformations from one direction to another, *i.e.* $I \rightarrow \theta$ by using attribute predictors [34] or $\theta \rightarrow I$ by synthetic rendering [22], [64], and learn a mapping network for the opposite direction.

3.2.2 Explicit Control over 3D Parameters

With 3D parameters obtained, many methods [22], [23], [30], [34], [64], [102] are developed to incorporate them as input control into a 2D generative model for controllable 3D-aware image synthesis. This section demonstrates how these methods introduce parameters and achieve explicit control through data collection, network design, and loss functions.

In MoFA [102], Tewari *et al.* (Mar 2017) use a CNN to project a face into the 3DMM space, followed by a differentiable renderer to synthesize the reconstructed face. The network is trained on a large collection of face images in a self-supervised manner. Inspired by the computer graphics pipeline, CONFIG [23] (May 2020) uses a set of parameters to represent and control desired factors. Blendshape values control facial expressions, Euler angles control head pose, and environment maps control the illumination. CONFIG has two encoders (E_R and E_S) that encode real face images I_R and the parameters $\theta : \{\theta_1, \dots, \theta_k\}$ of the synthetic images to a shared latent space \mathcal{Z} , which is factorised into elements that each part z_i corresponds to a different facial attribute controlled by θ_i . Each element z_i comes as the i -th parameter of $z \in \mathcal{Z}$ either from θ_i (encoded by E_S) or from a different real face image (encoded by E_R). They adopt

a two stage-training scheme to learn a disentangled latent space and produce photorealistic images.

Those based on StyleGANs [78], [103] either use a pre-trained StyleGAN model that keeps its weights fixed [22], [30] or make slight modifications to how 3D parameters are incorporated as conditions [34], [55]. StyleRig [22] and PIE [30] are two examples of using a pretrained StyleGAN. StyleRig (Apr 2020) trains a neural network, called RigNet, to inject a subset of parameters into a given StyleGAN latent code w . RigNet is a function $\text{rignet}(\cdot, \cdot)$ that maps a pair of StyleGAN code w and subset of 3DMM parameters θ to a new StyleGAN code w' , *i.e.* $w' = \text{rignet}(w, \theta)$. Several RigNets are trained, each dealing with a single mode of control (pose, expression, lighting). For self-supervised training, they introduce two key components: a learnable parameter regressor \mathcal{F} and a pretrained differentiable render layer \mathcal{R} . \mathcal{F} maps a latent code w to a vector of semantic control parameters θ : $\theta = \mathcal{F}(w)$. \mathcal{R} takes a parameter vector θ as input and generates a synthetic rendering $I_w = \mathcal{R}(\theta)$. StyleRig allows for multiple-attribute editing but only on synthetic facial images rather than real ones. In contrast, PIE (Sep 2020) uses a model-based face auto-encoder to replace \mathcal{F} and \mathcal{R} of StyleRig in support of real image editing.

Some methods inherit the main structure of Style-based generators and make slight modifications, mainly different on how the 3D parameters are incorporated as the condition. DiscoFaceGAN [55] (Apr 2020) proposes an unconditional 3D-aware method with controllability on four attributes: identity α , expression β , scene illumination γ , and face pose δ . Their model consists of two networks that learn the mapping 1) $V(\cdot)$ from z -space to θ -space; and 2) $G(\cdot)$ from θ -space to the image space. The latent code z is sampled from a standard normal distribution. The parameters θ is the concatenation of the four control factors $\theta := [\alpha, \beta, \gamma, \delta, \varepsilon]$ and the noise ε , which is the same of z for image diversity. They train four VAEs for α , β , γ , and δ on the θ samples extracted by using a off-the-shelf 3D face reconstruction method from real image set. Only the decoders are kept after the VAE training and denoted as $V_i, i = 1, 2, 3, 4$, for z -space to θ -space mapping. For training G , they sample $z = [z_1, \dots, z_5]$ from standard normal distribution, map it to θ , and feed θ to both G and the renderer to obtain a generated face x and a rendered face x' , respectively. They apply three types of losses for training: adversarial loss, imitative loss, and

TABLE 4
Overview of methods that incorporate 3D parameters to a 2D generative model.

Method	Publication	Control Factor	Supervision ($\theta \rightsquigarrow I$)
StyleRig [22]	CVPR 2020	3DMM parameters; θ	$I = \mathcal{R}(\theta)$
DiscoFaceGAN [55]	CVPR 2020	3DMM, SH, angle vector; θ	$\theta = \mathcal{F}(I)$
PIE [30]	TOG 2020	3DMM parameters; θ	$\theta = \text{MoFa}(G(w))$
CONFIG [23]	ECCV 2020	graphic parameters θ	synthetic images with θ
GAN-Control [34]	ICCV 2021	instutive representation y	$y_i = \mathcal{R}_i(G(z))$
3D-FM GAN [64]	ECCV 2022	a rendering $I_r(\theta)$ (equiv. to θ)	(image, rendering) pairs

contrastive loss. GAN-Control [34] (Jan 2021) builds on the StyleGAN2 [103] architecture. They divide the \mathcal{Z} and \mathcal{W} latent spaces to $N + 1$ separate sub-spaces, in accordance with N control attributes and one residual one for non-concerned information. The original StyleGAN2 architecture is changed from a single mapping network ($w = f(z)$), implemented as an eight-layered MLP) to each control z_i having its own $f(\cdot)$ so that $w_i = f(z_i)$. The combined latent vector (concatenation of the sub-vectors), w , is then fed into the generator G . To enable explicit control over each attribute, they use contrastive learning for disentanglement. Given a set of pretrained attribute predictors $\{\mathcal{R}_i\}_{i=1}^N$, they extract intermediate features as the attribute information from sampled images $G(z)$ and use them to calculate the distances during training. To support explicit control during inference, they further train N encoders $\{E_k\}_{k=1}^N$, each to map a human-interpretable attribute representation y^k to a latent code w^k . They use the attribute predictors to label the randomly-sampled images as the training data. Different from GAN-Control [34], in 3D-FM GAN [64], Liu *et al.* (Aug 2022) change StyleGAN G to make it conditional on a given image and a rendering. They estimate the lighting and 3DMM parameters of the face as the 3D parameters θ . These θ are not directly incorporated into G as the explicit control signal but are used instead to generate a rendering $I_r(\theta)$ of the same given image $I(\theta)$, which leads to a paired dataset. The resulting pairs $\{I(\theta), I_r(\theta)\}$ are used for reconstruction training, and $\{I(\theta_i), I_r(\theta_j)\}$ with different attributes of the same identity are for disentangled training.

3.3 Introducing 3D prior knowledge as Constraints

This category of studies facilitate the learning of 3D consistency by utilizing one or more kinds of 3D prior knowledge as constraints, such as shape [15], [26], [104], albedo [92], [105], normal [105], and depth [19], [52], [92]. Both § 3.2 and this section aim to make a 2D generative model, especially GAN, 3D-aware. § 3.2 focuses on the methods that incorporate 3D prior knowledge to 2D GANs for explicit control, while this section emphasizes those methods that introduce 3D-aware components into 2D GANs and use 3D prior knowledge as constraints for training. In addition to whether to introduce explicit 3D parameters as inputs, the slight difference between them is also reflected in the different concepts of dataset usage and network structure design. The former is able to control each of the desired attributes because of introducing 3D parameters as control factors but it lacks explicit geometry and texture as holistic 3D supervision, which leads to multi-view inconsistencies. The latter introduces 3D-aware components into 2D generative models (mostly GANs) and uses 3D prior knowledge (e.g. predicted depth from a off-the-shelf depth estimation method) to constrain the training process, resulting in a

degree of consistency but in the meantime a lack of fine-grained control. The two types of methods are not mutually exclusive. In addition to introducing 3D parameters to improve controllability, a few methods also implement 3D constraints to improve consistency across multiple views.

3.3.1 3D Prior Knowledge

Basically, the intrinsic components used to describe the physical world can be used here as priors, including but not limited to shape (surface, depth, and normal), material (albedo, reflectivity and shininess), and lighting (direction, intensity). We introduce in § 2.1 some common shape representations. Albedo, also referred to as reflection coefficient, is a measure of how reflective a surface is. It is either determined by a value between 0 and 1 or a percentage value. The more reflective a surface is, the higher the albedo value. A surface normal, or simply normal, to a surface at each point is a vector perpendicular to the tangent plane of the surface at that point. Normals represent the curvature of the object and can be used for reflecting light. Depth is the distance between the camera and the object at each pixel. They all contain geometric contextual features. There is a track of studies of intrinsic decomposition, which can be seen as a simplification of inverse rendering for general scenes, aiming to provide interpretable intermediate representations from images. There are also many methods specifically proposed to infer one specific environmental component, such as depth estimation, normal estimation, and light estimation. All these models can be potentially used as the training constraints for this category of methods.

3.3.2 Introducing 3D Components into 2D Models

With the chosen 3D priors, the next important decision for this kind of methods is to find a way of introducing 3D-aware components into their models and using 3D priors as training constraints. In S²-GAN [12], Wang *et al.* (Mar 2016) use a two-stage training for indoor scene synthesis: an unconditional GAN for structure (geometry) generates a surface normal map and the second GAN for style (appearance) takes this surface normal map as condition and outputs an image. VON [15] (Dec 2018) uses shape as the 3D prior and design a GAN based on 3D convolutional neural network to learn the geometry information. An unconditional shape GAN G_s first generates voxel grid shape s from a randomly sampled shape code z_s . The differentiable projection module then projects s to 2.5D sketches $s_{2.5D}$ at a sampled viewpoint z_v . The 2.5D sketches include both the object’s depth and silhouette. The texture network G_t finally adds realistic, diverse texture to these 2.5D sketches to generate 2D images: G_t takes $s_{2.5D}$ and another latent code z_t as input and outputs a 2D images. GIS [105] (Sep 2018) and NGP [26] (Feb 2021) utilize more than one 3D prior, such as albedo maps and normal maps, resulting in multiple 2D GANs to learn all the 3D attributes. In the above methods, 3D-aware components are used as intermediates, which are supervised by outputs from pretrained models. There are a few methods that only introduce 3D-aware components into 2D models without using 3D priors from pretrained models to constrain the training. For example, RGBD-GAN [19] (Sep 2019) generates two RGBD images with different camera parameters and then warps them to each other to ensure

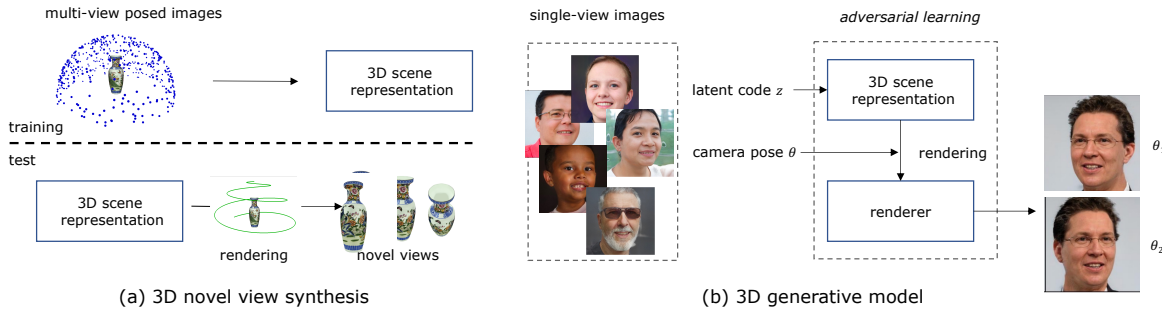


Fig. 5. The clarification of the defined terminology and the differences between 3D novel view synthesis methods (§ 4) and 3D generative models (§ 5). Both aim to generate multi-view-consistent and photo-realistic images, using a similar pipeline that learns the 3D representation first and then renders it. Their differences lie in the application scenarios and training data. 3D novel view synthesis (a) learns a 3D representation from *multiple views* of a scene. 3D generative models (b) learn to generate images from a collection of *single views*.

3D consistency. It learns to generate view-consistent images consistent from pure 2D image collections.

More recently, a few methods [52], [92] are build on top of StyleGAN architectures, either using a pretrained StyleGAN or adapting the vanilla design to their setting. They are also referred to as StyleGAN2-based 2.5D GANs in [48]. LiftedGAN [92] (Nov 2020) equips a pre-trained StyleGAN2 generator with five additional 3D-aware networks, which disentangle the latent space of StyleGAN2 into texture, shape, viewpoint, and lighting. These 3D components are then used for rendering. The proposed model is able to output both the 3D shape and texture, allowing explicit pose and lighting control. To control the viewpoint, DepthGAN [52] (Feb 2022) designs a dual-generator based on StyleGAN. The depth branch G_d takes as the input an uniformly sampled angle θ from range $[\theta_l, \theta_r]$ and a depth latent code, and synthesize a depth image at θ . The rgb branch G_r takes the intermediate feature maps of G_d as the conditions to acquire the geometry information. They use a pre-trained depth prediction model to get the corresponding depth image of each RGB image. A rotation consistency loss is introduced to enhance the multi-view consistency during training. The image synthesized under angle θ_1 is projected to a point cloud and re-projected to the 2D space under θ_2 , and compared with the image generated under θ_2 .

Despite impressive image quality, these methods still tend to produce 3D inconsistent faces under large expression and pose variations or scenes under different views due to the lack of a holistic 3D representation. They also inherit inconsistencies introduced by the pretrained model they use. For example, depth estimation methods, especially depth estimated from a single image, are known to suffer from the world-inconsistency. With the advances in differentiable rendering and implicit neural 3D representations, a recent line of work has explored photorealistic 3D-aware face or scene generation using *only* 2D image collections as the training data, *without any 3D supervision*. We introduce these studies in the following two sections.

4 3D NOVEL VIEW SYNTHESIS

This section mainly introduces methods under the single-scene overfitting (SSO) experiment, which aims to render novel views by learning a deep neural scene representation from multi-view image collections of a scene or object. These models are trained per-scene and are proposed for the task of 3D reconstruction and either novel view synthesis or free viewpoint rendering. This corresponds to

the three key components and improvement directions of recent algorithms: (better) deep 3D representation, (faster) rendering process, and (a smaller number of unlabeled and unstructured) training data (captured in a more real world environment). Methods introduced § 5 are also inspired by those in this section. Fig. 5 illustrates the general pipeline and comparison of the two kinds of methods. Both sections aim to infer a 3D scene representation from few images that can be used to render novel views. We categorize the related studies according to their underlying 3D representations (§ 4.1), training /inference acceleration (§ 4.2), and loose of constraints on the input data. The relaxation of constraints on input data expands the applicable scenario from a constrained environment to the real world, specifically 1) from a dense-view to a sparse-view image collection (§ 4.3); 2) from a calibrated to an uncalibrated image collection (§ 4.4); 3) from a single object to a large-scale scene (§ 4.5); and 4) from a static to a dynamic scene (§ 4.6). Tab. 5 is a comparison of 3D novel view synthesis methods using different 3D neural representations.

4.1 Different Neural Scene Representations

To render real-world scenes, early methods follow a computer graphics framework, which requires an pre-defined explicit model. Following that are generative methods for rendering novel views by concatenating target poses with latent codes or directly transforming views within the latent space. These methods lead to inconsistent results under different viewpoints. Instead, recent works have explored neural implicit methods, following the basic idea of representing a scene as a continuous function that maps a spatial location to a feature representation of learned scene properties at that spatial location. For example, DeepVoxels [14] (Dec 2018) is a learned representation that encodes the view-dependent appearance of a 3D scene without having to explicitly model its geometry. Scene Representation Networks (Jun 2019) [17] represent a scene implicitly as a continuous function $\Phi : \mathbb{R}^3 \rightarrow \mathbb{R}^n$ that maps a 3D world coordinate \mathbf{x} to a feature-based representation \mathbf{v} of the scene properties at that coordinate: $\mathbf{x} \mapsto \Phi(\mathbf{x}) = \mathbf{v}$. It consists of a 3D-structure-aware neural scene representation and a renderer that efficiently encapsulate both scene geometry and appearance. It is trained in an end-to-end manner from posed 2D images without 3D supervision. Given a scene representation Φ , a neural rendering maps Φ with camera parameters to an image. Most notably, Mildenhall *et al.* [5] (Mar 2020) propose Neural Radiance Fields (NeRF), which

achieve photorealistic quality by implicitly modeling the volumetric density and directional emitted radiance of a scene. It represents a scene as a continuous 5D vector-valued function whose input is a 3D location $x = (x, y, z)$ and a 2D viewing direction (θ, ϕ) , and whose output is an emitted color $c = (r, g, b)$ and a volume density σ . The color of any ray passing through the scene is rendered using principles from classical volume rendering [9]. These representations encode a scene in the 3D space, which can be referred to as the *3D-structured neural scene representations*.

To handle the prohibitively expensive rendering process of the 3D-structured neural scene representations, some methods learn to represent a scene with a latent vector from which novel views can be synthesized. Light Field Networks (LFN) [94] (Jun 2021) uses an auto-decoder to infer a latent code from input images, which then conditions an MLP to compute radiance values for rays of novel views. The rendering of LFN only requires one query per pixel, as opposed to hundreds of times required for rendering 3D-structured neural scene representations. This design enables real-time rendering and vast reduction in memory consumption. Scene Representation Transformer (SRT) [106] (Nov 2021) proposes a set-latent scene representation, which is processed by an encoder transformer the patch features extracted from images. The decoder transformer queries this representation to generate the pixel color for a view ray. They are also referred to as the *geometry-free approaches* as they do not encode a scene in the 3D space as opposed to the aforementioned methods. Some (*i.e.*, CodeNeRF [107], NeRF-VAE [108]) combine such global latent scene representation with NeRF, leading to an advantage of generalization for the sparse input view setting.

The scene representations here mean those encode both appearance and geometry of the underlying 3D scenes. It is noteworthy that some related methods [3], [4], [109] are proposed for 3D shape reconstruction but model geometry only with no appearance information, meaning them not able to render images with photorealistic textures. Therefore, we do not categorize them as our target methods in this survey. But it would be beneficial to pay attention to those works as these representations can also be used for the 3D-aware image synthesis task. They can be introduced as the geometric representation along with a textural representation (*e.g.*, Texture Field [110]) for 3D image synthesis.

NeRF [5] works for a small static scene and requires sufficient camera coverage / diversity over repeated observations. In addition, the costly sampling and queries in volume rendering make training and inference cumbersome. Several extensions have been proposed to mitigate shortcomings, including ones to accelerate rendering, handle color variations [75], optimize camera poses [40], be generalizable to new scenes [108], perform well with sparse or even few images [33], and accommodate large-scale [47] or dynamic scenes [111]. Similar to the dominance of NeRF-based representations in § 5, this section mainly focuses on NeRFs and their variants.

4.2 Speed-up Training and Inference

Most attempts to accelerate NeRF [5] can be classified into two categories. The first category [36], [38], [112], [113], [114] trains, precomputes, and stores NeRF MLP evaluation

results into more easily accessible data structures. This only increases inference speed. The second category [10], [54], [115], [116] usually jointly optimize a separate scene feature and a decoder MLP in a mutually beneficial manner, which can improve both training and inference speed.

In the first category, SNeRG [112] (Jul 2020) stores pre-computed diffused color, density, and feature vectors on a sparse voxel grid (referred to as baking in the paper). During evaluation, an MLP is used to produce specular color, which, combined with the specular colors alpha composited along the ray, produced the final pixel color. FastNeRF [38] (Mar 2021) factorizes the color function into the inner product of the output of the direction position dependent MLP and the output of a direction-dependent MLP. This allows FastNeRF to easily cache color and density evaluation in a dense grid of the scene. KiloNeRF [36] (Mar 2021) separates the scene into thousands of cells, and trains independent MLPs for color and density predictions on each cell. These thousands of small MLPs are trained using knowledge distillation from a large pretrained teacher MLP.

In the second category, Neural Sparse Voxel Fields (NSVF) [10] (Jul 2020) models a scene as a set of radiance fields bounded by voxels. Feature representations are obtained by interpolating learnable features stored at voxel vertices, which are then processed by a shared MLP to compute color and density. NSVF uses sparse voxel intersection-based point sampling for rays. This strategy is much more efficient than dense or hierarchical sampling. Instant-NGP [54] (Jan 2022) greatly accelerates NeRF model training and inference. They propose a parametric multi-resolution hash encoding that has been trained simultaneously with NeRF model MLPs. Further ray marching techniques are employed, such as exponential stepping, empty space skipping, and sample compaction. These techniques are also often used in other methods to further improve training and inference speed in conjunction.

In the following sections, we introduce the efforts of follow-up works to reduce the constraints on the input data from a constrained environment to in-the-wild real world.

4.3 From Dense to Sparse

The baseline NeRF requires a lengthy per-scene optimization on densely captured images. It suffers from overfitting to individual views and non-sensible scene geometry if there are not enough training samples. The learned radiance field only represents a single structure and cannot generalize across novel geometries. This makes it impractical for novel scenes with only a few available images. Several data-efficient NeRF extensions [33], [70], [107], [108], [117], [118] have been proposed to reconstruct radiance fields from just one or a few nearby input images. These methods rely on explicit 3D-to-2D projections of samples along the rays to gather features extracted from CNNs, which are then aggregated by a neural network for each point [33], [119], [120], or into a voxel grid [70]. In this way, these networks can be pre-trained, and then applied to novel scenes without optimization or additional per-scene fine-tuning. PixelNeRF [33] (Dec 2020) proposes to condition a NeRF on image inputs, which allows the network to be trained across multiple scenes to learn a scene prior, enabling it to perform novel view synthesis in a feed-forward manner

from a sparse set of views (as few as one). PixelNeRF can be trained on a set of multi-view images, allowing it to generate plausible novel view synthesis from very few input images without test-time optimization. MVSNeRF [70] (Mar 2021) uses a deep 2D CNN to extract features of input images, warps each feature map to the reference view, and constructs the cost volume from the warped feature maps. The 3D CNN is applied to reconstruct a neural encoding volume with per-voxel neural features, which are then used to regress color and density. MVSNeRF can generalize across scenes and generate photorealistic novel view results given only three nearby input views. NeRF-VAE [108] (Apr 2021) uses a scene function, which is shared between scenes and conditioned on a per-scene latent code. The scene function contains shared information (e.g. available textures and shapes or properties of common elements), while the latent code contains scene-specific information (e.g. object position and category, lighting, or colour). NeRF-VAE is able to infer the structure of an unknown scene from very few input views. CodeNeRF [107] (Sep 2021) learns to disentangle shape and texture with separate geometry and appearance codes. During inference, given a single unposed image of an unseen object, CodeNeRF jointly optimizes the geometry and appearance codes, as well as the camera pose. Unseen objects can first be reconstructed from the given image and then rendered to a novel view. Aside from NeRF, some methods based on other representations are also with generalization capabilities, e.g. SRT [106] and LFN [94]. In contrast to methods requiring explicit geometric inductive biases introduced by volume rendering, these *geometry-free approaches* have achieved results competitive with 3D-aware methods in the “few-shot” setting.

4.4 From Calibrated to Uncalibrated

For training NeRFs, most methods use images captured in a controlled environment (constrained) with known camera parameters (posed). However, real-life photographs of the same scene often do not have intrinsic and extrinsic camera poses available and may contain per-image appearance variations due to lighting, weather, as well as transient or moving objects. We refer to such scenarios as *uncalibrated*.

Camera poses can be acquired by COLMAP [65], which is used in many NeRF models. Recent methods propose to build NeRF models without precomputed camera pose [35], [40], [73], [121], [122]. Instead, they jointly estimate camera poses alongside the NeRF training, which is formulated as an offline structure from motion (SfM) problem or an on-line simultaneous localization and mapping (SLAM) problem. For example, NeRF- [35] (Feb 2021) jointly optimizes the camera parameters and scene representation, eliminating the need of pre-computing camera parameters, while achieving view synthesis results on par with the COLMAP-enabled NeRF baseline. However, due to limitations with pose initialization, NeRF- is suited for front-facing scenes. Bundle-Adjusted Neural Radiance Field (BARF) [40] (Apr 2021) also builds NeRF and estimates camera poses simultaneously. BARF also uses a coarse-to-fine registration by adaptively masking the positional encoding. SCNeRF [73] (Aug 2021) introduces a camera calibration model, which optimizes not only unknown poses but the camera intrinsic for non-linear camera models such as fish-eye lens.

Per-image appearance variations may exist in real-world images due to changes in lighting, weather [29], and transient objects [123]. NeRF models need improvement to train on these images. This is especially important when applying NeRF to a large-scale scene, where images can only be captured over months under different environmental conditions. For training with unconstrained photo collections, Martin-Brualla *et al.* [29] (Aug 2020) propose NeRF in the Wild (NeRF-W). The density MLP keeps fixed for all images in a scene while the color MLP is conditioned on a per-image appearance feature. Transient objects’ color and density functions are predicted by an additional MLP conditioned on per-image transient features. Generative latent optimization is used to construct these latent features. Based on the efforts of training NeRFs using unconstrained images, many methods extend the applicable scenarios from a small scene to a large-scale urban or city scene.

4.5 From Small to Large-scale

Several methods [47], [53], [125], [126] apply NeRF-based 3D reconstruction and novel view synthesis to urban-level outdoor environments. Urban Radiance Field [47] (Nov 2021) makes three modifications to tailor NeRF model to the street view setting and to tackle the challenges. To compensate for the sparsity of viewpoints in such large-scale and complex scenes, they use sparse multi-view images supplemented by asynchronously captured LiDAR data as input. To address exposure variation between captured images, they estimate an affine color transformation for each camera as the automatic compensation for varying exposure. To provide a well-defined supervision signal for camera rays pointing at the sky area, they segment sky pixels and define a separate dome-like structure. Mega-NeRF [127] (Dec 2021) performs urban-scale reconstruction and novel view synthesis from aerial drone images. It uses the inverse sphere parameterisation of NeRF++ [31] to separate background / foreground and incorporates the per-image appearance code of NeRF-W [29]. An ellipsoid is used to better fit the aerial point of view. An urban scene is divided into cells that each has a NeRF module. Each module is trained only on images with potentially relevant pixels. Colors and densities are first coarsely rendered and then refined dynamically through additional model sampling. Block-NeRF [53] (Feb 2022) scales NeRF to render city-level scenes spanning multiple blocks by decomposing the scene into independently trained NeRFs. In this way, the rendering time is decoupled from scene size, allowing the rendering of arbitrary large environments as well as per-block environment updates. To handle data collected over months under different environmental conditions, Block-NeRF is implemented with several modifications: 1) adding appearance code, pose refinement, and controllable exposure to each separate NeRF, and 2) introducing a procedure of appearance alignment to allow the seamless combination of adjacent NeRFs. This design allows Block-NeRF to render entire neighborhoods of San Francisco. To enable rendering across drastically-varied scales (from 6,300 m to 290 m), BungeeNeRF [125] (Dec 2021) proposes a progressive neural radiance field. In each training stage, the training set is gradually expanded by one closer scale, and the model is synchronously grown by multiple output heads for different levels of detail.

TABLE 5

Comparison of 3D novel view synthesis methods. The rows indicate whether each method 1) has been demonstrated to work with real world data, 2) is generalizable from a training set to novel scenes, 3) performs real-time inference, 4) works with very sparse (one or few) input images and 5) unknown camera poses, 6) supports images with appearance variations, 7) handles dynamic scenes, or 8) accommodates large-scale scenes.

	3D-structured neural scene representation																	Geometry-free				
	NeRF-based																	Others				
	NeRF [5]	FastNeRF [36]	NeRF-W [29]	BARF [40]	DietNeRF [117]	GRF [119]	IBRNet [120]	PixelNeRF [33]	MVSNeRF [70]	CodeNeRF [107]	NeRF-VAE [108]	BlockNeRF [53]	URF [47]	D-NeRF [93]	Nerfies [124]	3DiM [95]	DeepVoxels [14]	SRN [17]	DVR [7]	LFN [94]	SRT [106]	
1) Real-world data	✓	✓	✓	✓	✓	✓	✓	✓	✓	✓	✓	✓	✓	✓	✓	✓	✓	✓	✓	✓	✓	
2) Generalization	×	×	×	×	×	×	×	×	×	×	×	×	×	×	×	×	×	×	×	×	×	
3) Real-time	×	✓	×	×	×	×	×	×	×	×	×	×	×	×	×	×	×	×	×	×	×	
4) Few images	×	×	×	×	✓	×	✓	✓	✓	✓	✓	✓	✓	✓	✓	✓	✓	✓	✓	✓	✓	
5) Pose-free	×	×	×	✓	×	×	×	×	✓	✓	✓	✓	✓	✓	✓	✓	✓	✓	✓	✓	✓	
6) Varying appearance	×	×	✓	×	×	×	×	×	×	×	✓	✓	✓	✓	✓	×	×	×	×	✓	✓	
7) Large-scale	×	×	×	×	×	×	×	×	×	×	✓	✓	×	×	×	×	×	×	×	×	×	
8) Dynamic	×	×	×	×	×	×	×	×	×	×	×	×	✓	×	×	×	×	×	×	×	×	

4.6 From Static to Dynamic

In contrast to previous sections, geometries change when shape and motion are *non-rigid* and *deformable*. This section focuses on methods that extends NeRFs to a dynamic domain, such as a human body with movement or a face with expression [93], [111], [124], [128], [129], [130], [131], [132], [133], [134]. D-NeRF [93] (Nov 2020) takes time as an additional input, and splits the learning process into two main stages: one encoding the scene into a canonical representation and another mapping it into the deformed scene at a particular time. D-NeRF renders novel images, controlling both the camera view and the time variable. Neural Scene Flow Fields (NSFF) [131] (Nov 2020) models the dynamic scene as a time-variant continuous function of appearance, geometry, and motion. This representation is optimized through a neural network to fit the observed input views. Nerfies [124] (Nov 2020) extends NeRF by optimizing an additional continuous volumetric deformation field that warps each observed point into a canonical 5D NeRF. Inspired by principles of geometry processing and physical simulation to NeRF-like models, they propose an elastic regularization of the deformation field to improve robustness. Nerfies can turn casually-captured selfie photos or videos into a deformable NeRF, which allows for photorealistic renderings of the subject from arbitrary viewpoints. Non-Rigid Neural Radiance Fields (NR-NeRF) [132] (Dec 2020) is a reconstruction and novel view synthesis approach for general non-rigid dynamic scenes. It takes images of a dynamic scene (*e.g.*, from a monocular video) as input, and creates a high-quality space-time geometry and appearance representation. HyperNeRF [129] (Jun 2021) extends the canonical space in Nerfies to a higher dimension, and adds an additional slicing MLP to describe the 3D representation using ambient space coordinates. The canonical coordinate and ambient space coordinate are then used to condition baseline NeRF models’ density and color MLPs. HyperNeRF achieves excellent results in synthesizing views when scenes contain topological changes, such as a person opening the mouth and a banana being peeled. CoNeRF [134] (Dec 2021), built on HyperNeRF, allows sliders to easily edit face images. Slider values are provided to an MLP-parameterized per-attribute Hypermap deformation field. It achieves remarkable results, showing broad commercial applications for virtual human avatars.

5 3D-AWARE GENERATIVE MODELS

Inspired by 3D novel view synthesis methods, follow-up works introduce the efficient and expressive neural scene representations, especially INR to the field of 2D generative image synthesis, leading to a new paradigm called *3D-aware generative models* [2], [28]. These methods do not assume a large number of posed images of a single scene. Instead, they learn a model for synthesizing novel scenes by training on unlabeled and unposed single-view images without 3D supervision. These 3D-aware generative models follow a similar experimental setting as their 2D counterparts, *i.e.*, generating high quality photorealistic results from single-view image datasets, with an extra goal to ensure 3D consistency across multiple views. 3D GANs, an outstanding representative of 3D-aware generative models, usually utilize an adversarial framework to learn these representations in an unsupervised manner. In this section, we first introduce the unconditional 3D-aware generative networks based on different neural scene representations in § 5.1. We especially emphasize their efforts towards: 1) learning efficient and expressive geometry and appearance representations (§ 5.1.1); 2) developing accelerated and view-consistent rendering algorithms (§ 5.1.2); and 3) real-time and user-interactive editing (§ 5.1.3). We then present conditional 3D-aware generative models [57], [61], [71], [135], [136], [137] in § 5.2.

In 2D generative models, “unconditional” methods are referred to as those merely inputting latent codes that are sampled from a prior distribution. In this survey, we use “unconditional” 3D-aware generative models to refer to those using latent codes and camera positions as input. In some cases, the camera positions could also be generated from the randomly-sampled latent codes instead of human-understandable control factors. Those taking other inputs, especially image, text, semantic label, or sketch, are the conditional ones. The majority of methods in this part belong to the category of GANs. Some use generative latent optimization [46], [138] instead of adversarial training [139]. Other kinds of generative models, especially diffusion models [140], [141], which have proven extremely effective in generating high-quality images in recent years, have not yet been widely applied to 3D-aware image synthesis. Only very few recent studies are based on diffusion models [95] for 3D novel view synthesis. These generative models are expected to catch up in the near future.

Here is a clarification of the defined terminology and the differences between the two kinds of methods in § 4 and in this section. Both aim to generate multi-view-consistent and photorealistic images, using a similar pipeline that first learns the 3D representation and then renders it from that viewpoint (see Fig. 5). It is their application scenarios and training data that differentiate the two kinds of methods. As with their 2D counterparts, 3D-aware generative models generate images from a collection of single views, while 3D novel view synthesis learns a 3D representation from multiple views of a scene. The term *3D-aware generative models* may also be used to refer to 3D novel view synthesis methods, but this survey uses this term only in reference to the methods trained on single view images.

5.1 Unconditional 3D Generative Models

Like 2D GANs, 3D-aware GANs have recently achieved tremendous breakthroughs in terms of image quality and editability for 2D image synthesis, with the extra goal of 3D consistency by introducing explicit camera control. These methods can be formulated in the form of $I = f(z, \theta)$, where the noise vector z is for appearance and θ means camera pose. Towards editable, high-resolution, and view-consistent image synthesis, proposed methods mainly work on two key components: 1) to learn efficient and expressive representations of geometry and appearance; 2) to develop accelerated and view-consistent rendering algorithms. Some methods are proposed to facilitate user-interactive editing.

5.1.1 Efficient and Expressive Representations

Early 3D GANs adopt voxel-based representation. For example, PrGANs [13] (Dec 2016) and VON [15] (Dec 2018) first learn an explicit shape and render images at different viewpoints. They are trained under 3D supervision (as such they are also categorized into § 3.3). PlatonicGAN [142] (Nov 2018) learns a generative 3D model from an unstructured collection of 2D images. The learned shape and its rendered images are limited to low resolutions and coarse detail due to the computational complexity. The approaches using deep-voxel representations [16], [20] can create finely-detailed images under different poses. HoloGAN [16] (Apr 2019) first uses 3D convolutions to learn a deep-voxel representation (in a canonical pose), then utilizes a rigid-body transformation (3D rotation) to transform this representation to a certain pose, and finally applies a projection unit to render an image. In contrast to HoloGAN, which learns 3D features directly for the entire scene, BlockGAN [20] (Feb 2020) learns 3D features for each object separately. It decomposes a 3D scene into a background and one or more foreground objects, each of which is represented by a noise vector z_i . This design disentangles a scene into separate objects and enables control over camera pose, lighting, and shadow. However, early voxel-based methods [13], [15], [16], [20], [142] fail to synthesize complex scenes and photorealistic details due to the limited grid resolutions. Their reliance on a learned black-box rendering leads to discretization artifacts, degrades view-consistency of the generated images, and makes generalization to unseen camera poses difficult. Liao *et al.* [42] (Dec 2019) use 3D primitives as abstract object representations and differentiable rendering to project the 3D representations onto the image plane where

a 2D generator transforms them into object appearances and composites them into a coherent image.

The limited expressiveness and efficiency of previous methods typically prevents them from synthesising complex scenes and photorealistic details. Therefore, INRs, especially NeRFs, which have proven to generate high-fidelity results in novel view synthesis, are introduced to 3D-aware generative models. To avoid the requirement of posed images, an increasing number of methods turn to utilize an adversarial framework to train a generative model for these representations from *unposed* images. The visualization results from COLMAP validate those methods showing greater 3D consistency than the voxel-based representations. GRAF [28] (Jul 2020) uses NeRF to represent the scene and an adversarial framework to train on unposed images. The generator takes camera matrix, camera pose, 2D sampling pattern, and shape/appearance codes as input and predicts an image patch. The discriminator compares the synthesized patch to a real patch extracted from a real image. One significant modification is that GRAF makes NeRF conditioned on two additional latent codes: a shape noise and an appearance noise. A follow-up work pi-GAN [2] (Dec 2020) differs from GRAF in three ways on network architecture and training strategy: 1) pi-GAN uses SIREN [143] as the choice of scene representation rather than a positionally-encoded ReLU MLP [5]; 2) pi-GAN leverages a StyleGAN-inspired mapping network to condition layers in the SIREN on a single input noise code through feature-wise linear modulation (FiLM) instead of conditioning on two additional shape/appearance codes; 3) pi-GAN follows ProgressiveGAN [77] where discriminator grows progressively rather than a patch-based discriminator. Built similarly to pi-GAN, LOLNeRF [46] (Nov 2021), which is capable of single-shot view synthesis of human faces, uses generative latent optimization [138] instead of adversarial training [139]. GIRAFFE [32] improves the BlockGAN [20] framework by replacing the voxel-based representation and 3D-to-2D projection with a NeRF-based compositional 3D scene representation and a neural rendering pipeline. It can rotate, translate, scale each object and change camera poses but with compromised image quality and resolution.

Compared to 2D generative models, these models take much more calculations to render an image (speed) and require much more memory during training to cache intermediate results (memory). Computational constraints limit the rendering resolutions and quality. For high-quality image synthesis (towards 512×512 and beyond), recent methods turn to find more efficient and expressive representations of geometry and appearance, improve the training efficiency, or the combination of both. We focus on learning efficient and expressive representations as follow in this subsection, leaving later parts to the next subsection.

CIPS-3D [44] (Oct 2021) adopts a shallow NeRF network (containing only three SIREN blocks) to represent 3D shape and a deep 2D INR network to synthesis high-fidelity appearance. Inspired by recent progress in 3D surface reconstruction, GOF [45] (Nov 2021) combines implicit surfaces and radiance fields. They reinterpret the alpha values in the rendering equation as occupancy representations and reformulate generative radiance fields by predicting alpha values instead of volume densities. EG3D [48] (Dec 2021)

proposes a tri-plane hybrid 3D representation, formulated from explicit features of StyleGAN2 generator. They align explicit features along three axis-aligned orthogonal feature planes and query any 3D position by projecting it onto each of the three feature planes, resulting in an aggregated 3D feature. The aggregated features are then interpreted as color and density by an additional lightweight decoding network. This tri-plane representation is 3 to 8 times faster than an implicit Mip-NeRF [37] network and only requires a fraction of its memory. A super-resolution module upsamples and refines raw neurally rendered images. VolumeGAN [51] (Dec 2021) explicitly learns a structural representation and a textural representation. It learns a feature volume to represent the underlying structure, which is transformed into a feature field based on a NeRF-style model. The feature field is then aggregated into a 2D feature map as the textural representation. A neural renderer is finally used for appearance synthesis. StyleSDF [50] (Dec 2021) merges a SDF-based 3D representation into the 2D StyleGAN generator. This framework consists of two main components: a backbone conditional SDF volume renderer and a StyleGAN generator. The renderer takes in a latent code and camera parameters, queries points and view directions within the volume, and projects 3D surface features onto 2D views. To overcome the drawbacks of GIRAFFE and inherit its 3D controllability, a follow-up work GIRAFFE-HD [144] (Mar 2022) leverages a style-based neural renderer, generates the foreground and background independently, and stitches them together to composite a coherent final image. It enforces semantic disentanglement and 3D consistency through training constraints. In contrast to previous methods, VoxGRAF [59] (Jun 2022) adopts a 3D-aware GAN based on a sparse scene representation that allows for efficient rendering. It parameterizes the radiance field on a sparse voxel grid rather than using a coordinate-based MLP and predicts colors and density values on this sparse voxel grid using volume rendering. GMPI [62] (Jul 2022) makes a classical 2D GAN, *i.e.* StyleGAN2, 3D-aware by only introducing 1) a multiplane image style generator branch which produces a set of alpha maps conditioned on their depth; and 2) a pose conditioned discriminator.

5.1.2 Efficient and Consistent Rendering Algorithms

Early studies [16], [20] use simple 3D-to-2D projections for rendering. Such operations fail to produce high-quality images with fine-grained details and are restricted to representing poses in the training dataset. For higher rendering quality, recent methods adopt the state-of-the-art neural volume rendering techniques. GRAF [28] and pi-GAN [2] implement a discretized form of the volume rendering equation and uses the stratified and hierarchical sampling approach introduced by NeRF. The neural volume rendering approach has several advantages over previous 3D-to-2D projections: 1) producing images with fine details and high resolutions and 2) allowing for explicit control over camera pose, focal length, aspect ratio, and other parameters. Despite the advantages, the volume integrations approximated by sampling points along viewing rays are still costly for both training and inference. Some methods render the 3D representation directly at the final image resolution [2], [59]. Due to the high memory and computation cost of volume

rendering, direct rendering at target resolution is not efficient and struggles to generate images at high-resolution (512×512 and beyond). Some recently-developed methods make use of a two-stage rendering process [1], [32], [48], [50], [51] or develop efficient volume rendering strategy [43], [44], [49] for high-resolution image generation. Meanwhile, aimed to reduce view-inconsistent artifacts brought by the 2D renderers, they adopt different strategies such as NeRF path regularization [1] and dual discriminators [48].

Two-stage Rendering Process: To high-resolution image generation, some methods adopt a two-stage rendering process. Typically, they first generate a feature map at a low resolution and then employ upsampling in 2D space to progressively increase into the required high resolution. Niemeyer *et al.* [32] improve training and rendering efficiency by combining NeRF with a ConvNet-based renderer. Similarly, Chan *et al.* [48] perform the majority of the training at a rendering resolution of 64×64 and gradually increase the resolution, pixel-by-pixel, to 128×128, which are fed into a super-resolution module to produce images at the target resolution. However, these pixel-wise learnable upsamplers sacrifice view consistency and impair the quality of the learned 3D geometry due to network designs. In contrast, non-learnable upsamplers that interpolate the feature map with pre-defined lowpass filters (*e.g.* bilinear interpolation) produce smoother results but lead to non-removable bubble artifacts. In StyleNeRF [1], the two approaches are combined to balance quality and consistency.

Despite that upsampler scales the intermediate result to high resolution, it comes with two severe limitations: 1) the texture and shape change as camera moves; 2) the geometry is represented in a low resolution ($\approx 64^3$), both resulting in a compromised multi-view consistency of a generated object. To overcome the above limitations of the two-stage rendering, Skorokhodov *et al.* [60] drop the upsampler and improve the patch-wise optimization strategy [28] to build a 3D generator. They redesign the discriminator by making it better suited to operating on image patches of variable scales and locations, along with changing the random scale sampling strategy from an annealed uniform to an annealed beta distribution. This allows the proposed EpiGRAF to converge 2-3 times faster than upsampler-based architectures despite the generator modeling geometry in full resolution.

Efficient Rendering Strategy: This part is categorized into two groups of approaches according to their adopted strategies. As for the first group, an expressive and efficient representation allows usage of a simplified sampling strategy [50] or a lightweight decoder [48]. In StyleSDF [50], using SDFs leads to higher view-consistency and expressiveness, even with a simplified volume sampling strategy. They sample N points from N evenly-sized bins of integration intervals instead of stratified sampling [1], [2], [5], [28], which reduces the number of samples by half. VoxGARF [59] accelerates the rendering from the perspective of spatial sparsity, where volume rendering yields a foreground image and an alpha mask. The second group aims to develop efficient sampling strategy [43], [45], [49]. They constrain the point sampling in a reduced space rather than anywhere in the volume. GRAM [49] proposes a manifold predictor \mathcal{M} to predict a reduced space for point sampling and radiance field learning. \mathcal{M} is a light-weight MLP that maps a point

\mathbf{x} to a scalar value s . The predicted scalar field gives N isosurfaces with a set of predefined levels (constant values $\{l_i\}$): $\mathcal{S}_i = \{\mathbf{x} | \mathcal{M}(\mathbf{x}) = l_i\}$. The rendering only samples points from intersections between the determined isosurfaces and a camera ray. Pan *et al.* [43] introduce a light-weighted surface tracking network S to estimate the rendered object surface. This saves rendering computations by just querying points near the predicted surface. The sample region shrinks from the entire volume to a narrow interval around the surface.

Consistent View Regularization: Optimizing the radiance fields from a set of 2D training images can encounter critical degenerate solutions in the absence of geometry constraints, leading to a multi-view inconsistency problem in NeRF-based generative models. Some methods propose multi-view regularizations on colors and shapes to improve photometric and geometric consistencies. Different strategies are adopted to reduce view-inconsistent artifacts brought by the 2D renderers [1], [43], [48], [56], [145]. For example, Gu *et al.* [1] propose a NeRF path regularization to enforce 3D consistency, which is implemented by sub-sampling high-resolution outputs and comparing them against the low-resolution image generated by NeRF. Chan *et al.* [48] propose a pose-conditioned dual discriminators with two modifications in traditional GAN discriminators. First, they pass the rendering camera intrinsics and extrinsics matrices to the discriminator as a conditioning label. Second, they take as the input the concatenation of the final result I_r and a low-resolution RGB image I'_r . They interpret the first three feature channels of a neurally rendered feature image as I'_r and bilinearly upsample it to the same size of I_r . This pose-conditioned dual discriminator is used in many follow-up studies. Shi *et al.* [145] design a geometry-aware discriminator, GeoD, to improve 3D-aware GANs. Besides the real/fake classification, they assign the discriminator an additional geometry branch, aiming to derive the shape-related information (*e.g.* depth and normal), which is employed as an extra signal to supervise the generator. Pan *et al.* [43] observe that small variations of shape could lead to similar RGB images that look equally plausible to the discriminator, as the color of many objects is locally smooth. This phenomenon is referred to as shape-radiance (color) ambiguity. To eliminate this problem, they propose a multi-lighting constraint, which is realized by modeling illumination explicitly and rendering with various lighting conditions. To overcome the same issue, MVCGAN [56] (Apr 2022) builds geometry constraints by optimizing multiple views jointly to ensure geometry consistency between views. They minimize re-projection loss between a primary image and a warped image, and integrate a stereo mixup module to encourage the warped image to be similar to a real image. Such scheme guarantees geometry constraints between different views and supports large pose variations.

5.1.3 User-interactive Editing

Plenty of approaches are proposed to facilitate user-interactive editing. They can change the background’s appearance independent of the foreground, translate or rotate the foreground object in 3D, and change the foreground object’s shape and color. For example, some methods [20], [32], [144] use multiple noise vectors z_i to represent the background and each foreground object. Unlike previous studies

that learn 3D features directly for the whole scene [16], they learn a 3D feature for each object, render separately, and stitch them together to composite a coherent final image. Such design disentangles a scene into separate objects and enables control over camera pose, lighting, and shadow.

Differently, Kwak *et al.* [63] (Jul 2022) design a layer-wise SUBspace in INR NeRF-based generator (SURF-GAN). Instead of being used represent the background and each foreground object, multiple noise vectors are injected layer-by-layer into NeRF-based SURF blocks, in which interpretable dimensions are captured in layers with sub-modulation vectors. SURF-GAN [63] includes several SURF blocks that take position and view direction as inputs to predict view dependent color. IDE-3D [61] (May 2022) enables local control of the facial shape and texture and supports real-time, interactive editing. It makes two key modifications based on [48] to enable such interactive disentangled editing. First, they take two (instead of one) codes respectively representing shape and texture, which gives 3D volumes of semantic and texture in the tri-plane representation. Second, they jointly render rgb images and semantic masks (instead of just rgb images) through the volume rendering. The dual discriminator is also changed accordingly to take as input the concatenation of rgb and semantic masks.

5.2 Conditional 3D Generative Models

The unconditional 3D GANs in § 5.1 typically lack the capability of performing precise attribute editing for real images. Similar to 2D counterparts, 3D-aware real image editing could either use pretrained 3D GANs via GAN inversion or train a 3D-aware model from scratch with additional inputs.

As an emerging technique to bridge the real and fake image domains, GAN inversion [96] plays an essential role in enabling pretrained GAN models for applications of real image editing. It inverts a real image into the latent space of a trained GAN model, which allows us to alter image attributes by varying the inverted code in the latent space (known as latent space traversals). For 3D-aware image editing, some rely directly on 2D GAN inversion and latent space traversal techniques, while others develop tools particularly for 3D GAN inversion. For example, ShadeGAN [43] (Oct 2021) could also be used to reconstruct a given image by performing GAN inversion. Such inversion with this method allows to obtain object properties from the image, such as shape, normal, albedo, and shading. FENeRF [135] (Nov 2021) has attempted to edit the local shape and texture in a facial volume by using an optimization-based GAN inversion. Lin *et al.* [137] (Mar 2022) propose a method for multi-view consistent video editing and animation based on 3D GAN inversion. They invert the video frames into the latent space of a pi-GAN by using pivotal tuning inversion (PTI) [146] and edit face attributes by using StyleFlow [97]. IDE-3D [61] adopts a hybrid GAN inversion approach. Given a facial image and its semantic label, it obtains the texture and semantic latent codes with corresponding encoders and uses them as the initialization PTI to obtain high-fidelity reconstruction. Editing is performed by drawing on inverted semantic masks.

Other methods target at pose-dependent views by training a 3D network conditioned on a single image.

Pix2NeRF [71] (Feb 2022) demonstrates that merely applying a learning-based GAN inversion technique (learning an encoder and keeping the generator fixed during training) is insufficient to obtain an accurate mapping from image to latent space with pi-GAN as the backbone. Instead, they train the the encoder jointly with a generator and a discriminator (both of the same architecture and procedure as in [2]). Once trained, given an input image, Pix2NeRF disentangles its pose and content and renders novel views of the content. Sem2NeRF [57] (Mar 2022) takes as input a single-view 2D semantic mask and outputs a NeRF-based 3D representation that can be used to render photorealistic images in a 3D-aware view-consistent manner. AutoRF [136] (Apr 2022) focuses on novel view synthesis of objects without background. This model consists of an encoder that extracts a shape and an appearance code from an object’s image, which can be decoded into an implicit radiance field operating in normalized object space and leveraged for novel view synthesis. Object images are generated from real-world imagery by leveraging machine-generated 3D object detections and panoptic segmentation.

6 DISCUSSION

Despite great advances in 3D-aware image synthesis, many challenges remain and its rapid growth is expected to continue. In the following, we provide an overview of the future directions, problems to solve, and trends to anticipate. Due to their unique characteristics, some limitations or future trends may only apply to certain categories of methods.

Quality: Unlike traditional graphic rendering, since implicit neural representations do not provide an explicit and holistic 3D shape for rendering, inconsistencies seems inevitable in the generated surface and texture under different viewpoints. Moreover, these strategies are introduced separately rather than endogenously as part of the method. We expect that in the future there will be more endogenous approaches to 3D-aware image synthesis that generates high-quality, high-resolution, multi-view-consistent images in real time, as well as high-quality 3D geometry.

Speed: There is typically a slow training and inference speed with 3D-aware image synthesis methods. Most attempts to accelerate training and inference time require extra memory for caching trained models or use additional voxel/spatial-tree based scene features. It is expected that future speed-based methods should develop memory-friendly frameworks as well as novel inclusive and learnable scene representations to accelerate training and inference.

Editability: In spite of the promising quality of the produced results, most methods are incapable of editing individual image components. In some methods, latent vectors are used at various points along the pipeline to control composition, shape, and appearance of images. The latent codes enable the model to control small changes in scene content, such as lighting or coloration, per image. Others allow additional input to change aspects of the scene, such as images, texts, semantic labels, or direct control parameters. The editability of 3D-aware image synthesis methods, however, still has plenty of room for improvement compared to their 2D counterparts.

Forensics: The success of recent generative models has led to many new applications, but also raised ethical and

social concerns, such as fraud and fabricated images, videos, and news (known as deepfakes). The ability to detect deepfakes is essential to preventing malicious usage of these models. Recent studies have shown that a classifier can be trained to distinguish deepfakes and generalize to unseen architectures. It may continue to be a cat-and-mouse game in the future, since generated images will become increasingly difficult to detect. Conversely, these images can also be utilized as the training data for identifying fakes.

Network Design: Most current methods rely on a 2D architecture design that introduces 3D representation, rendering, and multi-view regularization to make a 2D model 3D-aware. The majority of 3D-aware generative models use convolution-powered generative adversarial networks. In recent years, transformer-based 2D image synthesis methods have emerged corresponding to their counterparts in convolutional networks. Developing 3D-aware generative models that are built on transformers with lighter structures and lower computational demands remains to be explored. Since almost all the methods above are based on GANs, developing other generative models that are 3D-aware, especially diffusion models, is also a promising future direction.

Applicable Scenarios: Like their 2D counterparts, current 3D-aware image synthesis methods exhibit state-of-the-art performance within narrow image domains. In most cases, they either require per-scene training or are restricted to images of certain types and structures. Recent efforts have been made to generalize 2D GANs to complex scenarios. StyleGAN-XL [147], for example, scales StyleGAN to large datasets with multiple classes of objects. Self-Distilled StyleGAN [148] aims to use internet photo collections for training. These efforts can enable 3D-aware image synthesis for real-world scenarios, but the attendant computational complexity will need to be addressed.

Evaluation metrics: It remains to be explored whether there are any reliable metrics that can better evaluate the photorealistic and geometric quality of generated images. Image quality and diversity are mainly measured by general metrics used for generative models. The 3D consistency is determined by measuring the distances between (pseudo-)depth maps and the similarity between identities at different camera positions. However, considering the lack of real reference, these calculated values only partially reflect the stability of the generated results, but cannot reflect the distance from the real samples. There is still a lack of effective assessment tools to evaluate the difference between the predicted and expected outcomes in a more reliable and direct manner for 3D-aware image synthesis.

7 CONCLUSION

This paper presents a comprehensive overview of recent advances in generative 3D image synthesis. We propose a systematic taxonomy for 3D-aware image synthesis. Specifically, we categorize the existing approaches into three groups: 3D control of 2D generative models, 3D-aware generative models from single view image collections, and novel view rendering from multiple view image collections. We also identify some open problems on this topic to inspire future research. We hope that this timely and up-to-date survey will serve as a starting point for future research to help advance this emerging and challenging field.

REFERENCES

- [1] J. Gu, L. Liu, P. Wang, and C. Theobalt, "StyleNeRF: A style-based 3D aware generator for high-resolution image synthesis," in *ICLR*, 2022. 1, 4, 6, 7, 15, 16
- [2] E. R. Chan, M. Monteiro, P. Kellnhofer, J. Wu, and G. Wetzstein, "pi-GAN: Periodic implicit generative adversarial networks for 3D-aware image synthesis," in *CVPR*, 2021. 1, 4, 6, 7, 13, 14, 15, 17
- [3] L. Mescheder, M. Oechsle, M. Niemeyer, S. Nowozin, and A. Geiger, "Occupancy networks: Learning 3d reconstruction in function space," in *CVPR*, 2019, pp. 4460–4470. 2, 3, 11
- [4] J. J. Park, P. Florence, J. Straub, R. Newcombe, and S. Lovegrove, "DeepSDF: Learning continuous signed distance functions for shape representation," in *CVPR*, 2019, pp. 165–174. 2, 3, 11
- [5] B. Mildenhall, P. P. Srinivasan, M. Tancik, J. T. Barron, R. Ramamoorthi, and R. Ng, "Nerf: Representing scenes as neural radiance fields for view synthesis," in *ECCV*, 2020. 2, 3, 4, 5, 7, 10, 11, 13, 14, 15
- [6] S. Peng, M. Niemeyer, L. Mescheder, M. Pollefeys, and A. Geiger, "Convolutional occupancy networks," in *ECCV*, 2020. 3
- [7] M. Niemeyer, L. Mescheder, M. Oechsle, and A. Geiger, "Differentiable volumetric rendering: Learning implicit 3d representations without 3d supervision," in *CVPR*, 2020. 3, 4, 7, 13
- [8] W. E. Lorensen and H. E. Cline, "Marching cubes: A high resolution 3d surface construction algorithm," *SIGGRAPH*, 1987. 3
- [9] J. T. Kajiya and B. P. Von Herzen, "Ray tracing volume densities," *SIGGRAPH*, vol. 18, no. 3, pp. 165–174, 1984. 3, 11
- [10] L. Liu, J. Gu, K. Z. Lin, T.-S. Chua, and C. Theobalt, "Neural sparse voxel fields," in *NeurIPS*, 2020. 3, 11
- [11] S. Lombardi, T. Simon, J. Saragih, G. Schwartz, A. Lehrmann, and Y. Sheikh, "Neural volumes: Learning dynamic renderable volumes from images," *TOG*, 2019. 3
- [12] X. Wang and A. Gupta, "Generative image modeling using style and structure adversarial networks," in *ECCV*, 2016. 4, 7, 9
- [13] M. Gadelha, S. Maji, and R. Wang, "3d shape induction from 2d views of multiple objects," in *3DV*, 2017. 4, 7, 14
- [14] V. Sitzmann, J. Thies, F. Heide, M. Nießner, G. Wetzstein, and M. Zollhofer, "Deepvoxels: Learning persistent 3d feature embeddings," in *CVPR*, 2019, pp. 2437–2446. 3, 4, 5, 7, 10, 13
- [15] J.-Y. Zhu, Z. Zhang, C. Zhang, J. Wu, A. Torralba, J. Tenenbaum, and B. Freeman, "Visual object networks: Image generation with disentangled 3d representations," *NeurIPS*, 2018. 4, 7, 9, 14
- [16] T. Nguyen-Phuoc, C. Li, L. Theis, C. Richardt, and Y.-L. Yang, "HoloGAN: Unsupervised learning of 3D representations from natural images," in *ICCV*, 2019. 4, 6, 7, 14, 15, 16
- [17] V. Sitzmann, M. Zollhöfer, and G. Wetzstein, "Scene representation networks: Continuous 3d-structure-aware neural scene representations," *NeurIPS*, vol. 32, 2019. 4, 7, 10, 13
- [18] A. Jahanian, L. Chai, and P. Isola, "On the "steerability" of generative adversarial networks," in *ICLR*, 2020. 4, 6, 7
- [19] A. Noguchi and T. Harada, "RGBD-GAN: Unsupervised 3d representation learning from natural image datasets via rgbd image synthesis," in *ICLR*, 2020. 4, 7, 9
- [20] T. Nguyen-Phuoc, C. Richardt, L. Mai, Y.-L. Yang, and N. Mitra, "BlockGAN: Learning 3D object-aware scene representations from unlabelled images," in *NeurIPS*, 2020. 4, 6, 7, 14, 15, 16
- [21] A. Voynov and A. Babenko, "Unsupervised discovery of interpretable directions in the GAN latent space," in *ICML*, 2020. 4, 6, 7
- [22] A. Tewari, M. Elgharib, G. Bharaj, F. Bernard, H.-P. Seidel, P. Pérez, M. Zollhofer, and C. Theobalt, "StyleRig: Rigging StyleGAN for 3D control over portrait images," in *CVPR*, 2020. 4, 7, 8, 9
- [23] M. Kowalski, S. J. Garbin, V. Estellers, T. Baltrušaitis, M. Johnson, and J. Shotton, "Config: Controllable neural face image generation," in *ECCV*, 2020, pp. 299–315. 4, 7, 8, 9
- [24] H. Erik, H. Aaron, L. Jaakko, and P. Sylvain, "GANSpace: Discovering interpretable GAN controls," in *NeurIPS*, 2020. 4, 6, 7
- [25] Y. Shen, J. Gu, X. Tang, and B. Zhou, "Interpreting the latent space of GANs for semantic face editing," in *CVPR*, 2020. 4, 6, 7
- [26] X. Chen, D. Cohen-Or, B. Chen, and N. J. Mitra, "Towards a neural graphics pipeline for controllable image generation," in *CGF*, vol. 40, no. 2, 2021, pp. 127–140. 4, 7, 9
- [27] Y. Shen and B. Zhou, "Closed-form factorization of latent semantics in GANs," in *CVPR*, 2021. 4, 6, 7
- [28] K. Schwarz, Y. Liao, M. Niemeyer, and A. Geiger, "GRAF: Generative radiance fields for 3D-aware image synthesis," in *NeurIPS*, 2020. 4, 7, 13, 14, 15
- [29] R. Martin-Brualla, N. Radwan, M. S. Sajjadi, J. T. Barron, A. Dosovitskiy, and D. Duckworth, "Nerf in the wild: Neural radiance fields for unconstrained photo collections," in *CVPR*, 2021, pp. 7210–7219. 4, 7, 12, 13
- [30] A. Tewari, M. Elgharib, M. BR, F. Bernard, H.-P. Seidel, P. Pérez, M. Zollhofer, and C. Theobalt, "Pie: Portrait image embedding for semantic control," *TOG*, 2020. 4, 7, 8, 9
- [31] K. Zhang, G. Riegler, N. Snavely, and V. Koltun, "Nerf++: Analyzing and improving neural radiance fields," *arXiv preprint arXiv:2010.07492*, 2020. 4, 7, 12
- [32] M. Niemeyer and A. Geiger, "GIRAFFE: Representing scenes as compositional generative neural feature fields," in *CVPR*, 2021. 4, 6, 7, 14, 15, 16
- [33] A. Yu, V. Ye, M. Tancik, and A. Kanazawa, "pixelNeRF: Neural radiance fields from one or few images," in *CVPR*, 2021, pp. 4578–4587. 4, 7, 11, 13
- [34] A. Shoshan, N. Bhonker, I. Kviatkovsky, and G. Medioni, "GAN-control: Explicitly controllable GANs," in *ICCV*, 2021, pp. 14 083–14 093. 4, 7, 8, 9
- [35] Z. Wang, S. Wu, W. Xie, M. Chen, and V. A. Prisacariu, "NeRF-: Neural radiance fields without known camera parameters," *arXiv preprint arXiv:2102.07064*, 2021. 4, 7, 12
- [36] C. Reiser, S. Peng, Y. Liao, and A. Geiger, "Kilonerf: Speeding up neural radiance fields with thousands of tiny mlps," in *ICCV*, 2021, pp. 14 335–14 345. 4, 7, 11
- [37] J. T. Barron, B. Mildenhall, M. Tancik, P. Hedman, R. Martin-Brualla, and P. P. Srinivasan, "Mip-NeRF: A multiscale representation for anti-aliasing neural radiance fields," in *ICCV*, 2021, pp. 5855–5864. 4, 5, 15
- [38] S. J. Garbin, M. Kowalski, M. Johnson, J. Shotton, and J. Valentin, "FastNeRF: High-fidelity neural rendering at 200fps," in *ICCV*, 2021, pp. 14 346–14 355. 4, 7, 11, 13
- [39] M. Niemeyer and A. Geiger, "Campari: Camera-aware decomposed generative neural radiance fields," in *3DV*, 2021. 4, 7
- [40] C.-H. Lin, W.-C. Ma, A. Torralba, and S. Lucey, "BARF: Bundle-adjusting neural radiance fields," in *IEEE International Conference on Computer Vision (ICCV)*, 2021. 4, 7, 11, 12, 13
- [41] M. C. Bühler, A. Meka, G. Li, T. Beeler, and O. Hilliges, "VariTex: Variational neural face textures," in *ICCV*, 2021. 4
- [42] Y. Liao, K. Schwarz, L. Mescheder, and A. Geiger, "Towards unsupervised learning of generative models for 3D controllable image synthesis," in *CVPR*, 2020, pp. 5871–5880. 4, 7, 14
- [43] X. Pan, X. Xu, C. C. Loy, C. Theobalt, and B. Dai, "A shading-guided generative implicit model for shape-accurate 3d-aware image synthesis," in *NeurIPS*, 2021. 4, 7, 15, 16
- [44] P. Zhou, L. Xie, B. Ni, and Q. Tian, "CIPS-3D: A 3d-aware generator of gans based on conditionally-independent pixel synthesis," *arXiv preprint arXiv:2110.09788*, 2021. 4, 5, 14, 15
- [45] X. Xu, X. Pan, D. Lin, and B. Dai, "Generative occupancy fields for 3d surface-aware image synthesis," in *NeurIPS*, 2021. 4, 5, 7, 14, 15
- [46] D. Rebain, M. Matthews, K. M. Yi, D. Lagun, and A. Tagliasacchi, "LOLNeRF: Learn from one look," in *CVPR*, 2022. 4, 6, 13, 14
- [47] K. Rematas, A. Liu, P. P. Srinivasan, J. T. Barron, A. Tagliasacchi, T. Funkhouser, and V. Ferrari, "Urban radiance fields," in *CVPR*, 2022, pp. 12 932–12 942. 4, 11, 12, 13
- [48] E. R. Chan, C. Z. Lin, M. A. Chan, K. Nagano, B. Pan, S. D. Mello, O. Gallo, L. Guibas, J. Tremblay, S. Khamis, T. Karras, and G. Wetzstein, "Efficient Geometry-aware 3D Generative Adversarial Networks," in *CVPR*, 2022. 4, 5, 6, 7, 10, 14, 15, 16
- [49] Y. Deng, J. Yang, J. Xiang, and X. Tong, "GRAM: Generative Radiance Manifolds for 3D-Aware Image Generation," in *CVPR*, 2022. 4, 6, 7, 15
- [50] R. Or-El, X. Luo, M. Shan, E. Shechtman, J. J. Park, and I. Kemelmacher-Shlizerman, "StyleSDF: High-resolution 3d-consistent image and geometry generation," *CVPR*, 2022. 4, 5, 6, 7, 15
- [51] Y. Xu, S. Peng, C. Yang, Y. Shen, and B. Zhou, "3D-aware Image Synthesis via Learning Structural and Textural Representations," in *CVPR*, 2022. 4, 6, 7, 15
- [52] Z. Shi, Y. Shen, J. Zhu, D.-Y. Yeung, and Q. Chen, "3d-aware indoor scene synthesis with depth priors," in *ECCV*, 2022. 4, 5, 7, 9, 10

- [53] M. Tancik, V. Casser, X. Yan, S. Pradhan, B. Mildenhall, P. P. Srinivasan, J. T. Barron, and H. Kretzschmar, "Block-nerf: Scalable large scene neural view synthesis," in *CVPR*, 2022. 4, 5, 7, 12, 13
- [54] T. Müller, A. Evans, C. Schied, and A. Keller, "Instant neural graphics primitives with a multiresolution hash encoding," *TOG*, 2022. 4, 7, 11
- [55] Y. Deng, J. Yang, D. Chen, F. Wen, and X. Tong, "Disentangled and controllable face image generation via 3D imitative-contrastive learning," in *CVPR*, 2020, pp. 5154–5163. 4, 7, 8, 9
- [56] X. Zhang, Z. Zheng, D. Gao, B. Zhang, P. Pan, and Y. Yang, "Multi-view consistent generative adversarial networks for 3D-aware image synthesis," in *CVPR*, 2022. 4, 16
- [57] Y. Chen, Q. Wu, C. Zheng, T.-J. Cham, and J. Cai, "Sem2NeRF: Converting single-view semantic masks to neural radiance fields," in *ECCV*, 2022. 4, 7, 13, 17
- [58] A. Tewari, X. Pan, O. Fried, M. Agrawala, C. Theobalt *et al.*, "Disentangled3D: Learning a 3d generative model with disentangled geometry and appearance from monocular images," in *CVPR*, 2022, pp. 1516–1525. 4, 6
- [59] K. Schwarz, A. Sauer, M. Niemeyer, Y. Liao, and A. Geiger, "VoxGRAF: Fast 3d-aware image synthesis with sparse voxel grids," in *NeurIPS*, 2022. 4, 15
- [60] I. Skorokhodov, S. Tulyakov, Y. Wang, and P. Wonka, "EpiGRAF: Rethinking training of 3D gans," in *NeurIPS*, 2022. 4, 6, 7, 15
- [61] J. Sun, X. Wang, Y. Shi, L. Wang, J. Wang, and Y. Liu, "IDE-3D: Interactive disentangled editing for high-resolution 3D-aware portrait synthesis," in *SIGGRAPH Asia*, 2022. 4, 7, 13, 16
- [62] X. Zhao, F. Ma, D. Güera, Z. Ren, A. G. Schwing, and A. Colburn, "Generative multiplane images: Making a 2d gan 3d-aware," in *ECCV*, 2022. 4, 15
- [63] J.-g. Kwak, Y. Li, D. Yoon, D. Kim, D. Han, and H. Ko, "Injecting 3d perception of controllable nerf-gan into stylegan for editable portrait image synthesis," in *ECCV*, 2022. 4, 7, 16
- [64] Y. Liu, Z. Shu, Y. Li, Z. Lin, R. Zhang, and S. Kung, "3D-FM GAN: Towards 3d-controllable face manipulation," in *ECCV*, 2022. 4, 7, 8, 9
- [65] J. L. Schonberger and J.-M. Frahm, "Structure-from-motion revisited," in *CVPR*, 2016, pp. 4104–4113. 3, 12
- [66] A. Dai, A. X. Chang, M. Savva, M. Halber, T. Funkhouser, and M. Nießner, "ScanNet: Richly-annotated 3d reconstructions of indoor scenes," in *CVPR*, 2017, pp. 5828–5839. 3
- [67] A. X. Chang, T. Funkhouser, L. Guibas, P. Hanrahan, Q. Huang, Z. Li, S. Savarese, M. Savva, S. Song, H. Su *et al.*, "Shapenet: An information-rich 3d model repository," *arXiv preprint arXiv:1512.03012*, 2015. 3
- [68] R. Jensen, A. Dahl, G. Vogiatzis, E. Tola, and H. Aanaes, "Large scale multi-view stereopsis evaluation," in *CVPR*, 2014. 4, 5
- [69] A. Knapitsch, J. Park, Q.-Y. Zhou, and V. Koltun, "Tanks and temples: Benchmarking large-scale scene reconstruction," *TOG*, vol. 36, no. 4, pp. 1–13, 2017. 4
- [70] A. Chen, Z. Xu, F. Zhao, X. Zhang, F. Xiang, J. Yu, and H. Su, "Mvsnerf: Fast generalizable radiance field reconstruction from multi-view stereo," in *ICCV*, 2021. 5, 11, 12, 13
- [71] S. Cai, A. Obukhov, D. Dai, and L. Van Gool, "Pix2NeRF: Unsupervised conditional p-GAN for single image to neural radiance fields translation," in *CVPR*, 2022. 5, 6, 7, 13, 17
- [72] L. Yang, P. Luo, C. Change Loy, and X. Tang, "A large-scale car dataset for fine-grained categorization and verification," in *CVPR*, 2015, pp. 3973–3981. 5, 6
- [73] Y. Jeong, S. Ahn, C. Choy, A. Anandkumar, M. Cho, and J. Park, "Self-calibrating neural radiance fields," in *ICCV*, 2021. 5, 12
- [74] Y. Jin, D. Mishkin, A. Mishchuk, J. Matas, P. Fua, K. M. Yi, and E. Trulls, "Image matching across wide baselines: From paper to practice," *IJCV*, vol. 129, no. 2, pp. 517–547, 2021. 4, 5
- [75] R. Martin-Brualla, N. Radwan, M. S. Sajjadi, J. T. Barron, A. Dosovitskiy, and D. Duckworth, "Nerf in the wild: Neural radiance fields for unconstrained photo collections," in *CVPR*, 2021. 4, 5, 11
- [76] Z. Liu, P. Luo, X. Wang, and X. Tang, "Deep learning face attributes in the wild," in *ICCV*, 2015. 4, 6
- [77] T. Karras, T. Aila, S. Laine, and J. Lehtinen, "Progressive growing of GANs for improved quality, stability, and variation," in *ICLR*, 2018. 4, 6, 14
- [78] T. Karras, S. Laine, and T. Aila, "A style-based generator architecture for generative adversarial networks," in *CVPR*, 2019, pp. 4401–4410. 4, 6, 8
- [79] A. Dosovitskiy, G. Ros, F. Codevilla, A. Lopez, and V. Koltun, "CARLA: An open urban driving simulator," in *CoRL*, 2017. 4, 6
- [80] F. Yu, Y. Zhang, S. Song, A. Seff, and J. Xiao, "Lsun: Construction of a large-scale image dataset using deep learning with humans in the loop," *arXiv preprint arXiv:1506.03365*, 2015. 4, 6
- [81] J. Johnson, B. Hariharan, L. Van Der Maaten, L. Fei-Fei, C. Lawrence Zitnick, and R. Girshick, "CLEVR: A diagnostic dataset for compositional language and elementary visual reasoning," in *CVPR*, 2017, pp. 2901–2910. 4, 6
- [82] Y. Choi, Y. Uh, J. Yoo, and J.-W. Ha, "StarGAN v2: Diverse image synthesis for multiple domains," in *CVPR*, 2020. 6
- [83] T. Karras, M. Aittala, J. Hellsten, S. Laine, J. Lehtinen, and T. Aila, "Training generative adversarial networks with limited data," in *NeurIPS*, 2020. 6
- [84] T. Salimans, I. Goodfellow, W. Zaremba, V. Cheung, A. Radford, and X. Chen, "Improved techniques for training GANs," in *NeurIPS*, 2016. 5
- [85] M. Heusel, H. Ramsauer, T. Unterthiner, B. Nessler, and S. Hochreiter, "GANs trained by a two time-scale update rule converge to a local Nash equilibrium," in *NeurIPS*, 2017. 5
- [86] R. Zhang, P. Isola, A. A. Efros, E. Shechtman, and O. Wang, "The unreasonable effectiveness of deep features as a perceptual metric," in *CVPR*, 2018, pp. 586–595. 5
- [87] C. Szegedy, V. Vanhoucke, S. Ioffe, J. Shlens, and Z. Wojna, "Rethinking the inception architecture for computer vision," in *CVPR*, 2016, pp. 2818–2826. 5
- [88] J. Deng, W. Dong, R. Socher, L.-J. Li, K. Li, and L. Fei-Fei, "Imagenet: A large-scale hierarchical image database," in *CVPR*, 2009. 5
- [89] K. Simonyan and A. Zisserman, "Very deep convolutional networks for large-scale image recognition," in *ICLR*, 2015. 5
- [90] Z. Wang, A. C. Bovik, H. R. Sheikh, and E. P. Simoncelli, "Image quality assessment: From error visibility to structural similarity," *TIP*, vol. 13, 2004. 5
- [91] J. Deng, J. Guo, N. Xue, and S. Zafeiriou, "ArcFace: Additive angular margin loss for deep face recognition," in *CVPR*, 2019. 5
- [92] Y. Shi, D. Aggarwal, and A. K. Jain, "Lifting 2d stylegan for 3d-aware face generation," in *CVPR*, 2021, pp. 6258–6266. 7, 9, 10
- [93] A. Pumarola, E. Corona, G. Pons-Moll, and F. Moreno-Noguer, "D-NeRF: Neural radiance fields for dynamic scenes," in *CVPR*, 2021, pp. 10318–10327. 7, 13
- [94] V. Sitzmann, S. Rezkikov, B. Freeman, J. Tenenbaum, and F. Durand, "Light field networks: Neural scene representations with single-evaluation rendering," *NeurIPS*, 2021. 7, 11, 12, 13
- [95] D. Watson, W. Chan, R. Martin-Brualla, J. Ho, A. Tagliasacchi, and M. Norouzi, "Novel view synthesis with diffusion models," *arXiv preprint arXiv:2210.04628*, 2022. 7, 13
- [96] W. Xia, Y. Zhang, Y. Yang, J.-H. Xue, B. Zhou, and M.-H. Yang, "GAN inversion: A survey," *TPAMI*, 2022. 6, 16
- [97] R. Abdal, P. Zhu, N. Mitra, and P. Wonka, "StyleFlow: Attribute-conditioned exploration of StyleGAN-generated images using conditional continuous normalizing flows," *TOG*, 2021. 6, 8, 16
- [98] V. Blanz and T. Vetter, "A morphable model for the synthesis of 3d faces," in *SIGGRAPH*, 1999, pp. 187–194. 7, 8
- [99] Y. Hong, B. Peng, H. Xiao, L. Liu, and J. Zhang, "HeadNeRF: A real-time nerf-based parametric head model," in *CVPR*, 2022. 7
- [100] K. Sun, S. Wu, Z. Huang, N. Zhang, Q. Wang, and H. Li, "Controllable 3d face synthesis with conditional generative occupancy fields," in *NeurIPS*, 2022. 7
- [101] R. Ramamoorthi and P. Hanrahan, "An efficient representation for irradiance environment maps," in *SIGGRAPH*, 2001. 8
- [102] A. Tewari, M. Zollhofer, H. Kim, P. Garrido, F. Bernard, P. Perez, and C. Theobalt, "MoFA: Model-based deep convolutional face autoencoder for unsupervised monocular reconstruction," in *ICCV workshops*, 2017, pp. 1274–1283. 8
- [103] T. Karras, S. Laine, M. Aittala, J. Hellsten, J. Lehtinen, and T. Aila, "Analyzing and improving the image quality of StyleGAN," in *CVPR*, 2020. 8, 9
- [104] J. Wu, C. Zhang, T. Xue, B. Freeman, and J. Tenenbaum, "Learning a probabilistic latent space of object shapes via 3d generative-adversarial modeling," *NeurIPS*, vol. 29, 2016. 9
- [105] H. Abu Alhaja, S. K. Mustikovela, A. Geiger, and C. Rother, "Geometric image synthesis," in *ACCV*, 2018, pp. 85–100. 9
- [106] M. S. Sajjadi, H. Meyer *et al.*, "Scene representation transformer: Geometry-free novel view synthesis through set-latent scene representations," in *CVPR*, 2022, pp. 6229–6238. 11, 12, 13

- [107] W. Jang and L. Agapito, "CodeNeRF: Disentangled neural radiance fields for object categories," in *ICCV*, 2021. [11](#), [12](#), [13](#)
- [108] A. R. Kosiorek, H. Strathmann, D. Zoran, P. Moreno, R. Schneider, S. Mokrá, and D. J. Rezende, "NeRF-VAE: A geometry aware 3D scene generative model," in *ICML*, 2021. [11](#), [12](#), [13](#)
- [109] V. Sitzmann, E. Chan, R. Tucker, N. Snavely, and G. Wetzstein, "MetaSDF: Meta-learning signed distance functions," *NeurIPS*, vol. 33, pp. 10136–10147, 2020. [11](#)
- [110] M. Oechsle, L. Mescheder, M. Niemeyer, T. Strauss, and A. Geiger, "Texture fields: Learning texture representations in function space," in *ICCV*, 2019, pp. 4531–4540. [11](#)
- [111] G. Gafni, J. Thies, M. Zollhofer, and M. Nießner, "Dynamic neural radiance fields for monocular 4d facial avatar reconstruction," in *CVPR*, 2021, pp. 8649–8658. [11](#), [13](#)
- [112] P. Hedman, P. P. Srinivasan, B. Mildenhall, J. T. Barron, and P. Debevec, "Baking neural radiance fields for real-time view synthesis," in *ICCV*, 2021, pp. 5875–5884. [11](#)
- [113] A. Yu, R. Li, M. Tancik, H. Li, R. Ng, and A. Kanazawa, "Plenotrees for real-time rendering of neural radiance fields," in *ICCV*, 2021, pp. 5752–5761. [11](#)
- [114] T. Hu, S. Liu, Y. Chen, T. Shen, and J. Jia, "EfficientNeRF: Efficient neural radiance fields," in *CVPR*, 2022, pp. 12902–12911. [11](#)
- [115] D. B. Lindell, J. N. Martel, and G. Wetzstein, "Autoint: Automatic integration for fast neural volume rendering," in *CVPR*, 2021. [11](#)
- [116] L. Wu, J. Y. Lee, A. Bhattad, Y.-X. Wang, and D. Forsyth, "DIVER: Real-time and accurate neural radiance fields with deterministic integration for volume rendering," in *CVPR*, 2022. [11](#)
- [117] A. Jain, M. Tancik, and P. Abbeel, "Putting nerf on a diet: Semantically consistent few-shot view synthesis," in *ICCV*, 2021, pp. 5885–5894. [11](#), [13](#)
- [118] Y. Liu, S. Peng, L. Liu, Q. Wang, P. Wang, C. Theobalt, X. Zhou, and W. Wang, "Neural rays for occlusion-aware image-based rendering," in *CVPR*, 2022, pp. 7824–7833. [11](#)
- [119] A. Trevisan and B. Yang, "GRF: Learning a general radiance field for 3D representation and rendering," in *ICCV*, 2021, pp. 15182–15192. [11](#), [13](#)
- [120] Q. Wang, Z. Wang, K. Genova, P. P. Srinivasan, H. Zhou, J. T. Barron, R. Martin-Brualla, N. Snavely, and T. Funkhouser, "IBRNet: Learning multi-view image-based rendering," in *CVPR*, 2021, pp. 4690–4699. [11](#), [13](#)
- [121] S.-Y. Su, F. Yu, M. Zollhofer, and H. Rhodin, "A-NeRF: Articulated neural radiance fields for learning human shape, appearance, and pose," *NeurIPS*, 2021. [12](#)
- [122] Q. Meng, A. Chen, H. Luo, M. Wu, H. Su, L. Xu, X. He, and J. Yu, "GNeRF: GAN-based neural radiance field without posed camera," in *ICCV*, 2021, pp. 6351–6361. [12](#)
- [123] Y.-C. Guo, D. Kang, L. Bao, Y. He, and S.-H. Zhang, "NeRFReN: Neural radiance fields with reflections," in *CVPR*, 2022. [12](#)
- [124] K. Park, U. Sinha, J. T. Barron, S. Bouaziz, D. B. Goldman, S. M. Seitz, and R. Martin-Brualla, "Nerfies: Deformable neural radiance fields," in *ICCV*, 2021, pp. 5865–5874. [13](#)
- [125] Y. Xiangli, L. Xu, X. Pan, N. Zhao, A. Rao, C. Theobalt, B. Dai, and D. Lin, "BungeeNeRF: Progressive neural radiance field for extreme multi-scale scene rendering," in *ECCV*, 2022. [12](#)
- [126] D. Derksen and D. Izzo, "Shadow neural radiance fields for multi-view satellite photogrammetry," in *CVPR*, 2021. [12](#)
- [127] H. Turki, D. Ramanan, and M. Satyanarayanan, "MegaNERF: Scalable construction of large-scale nerfs for virtual fly-throughs," in *CVPR*, 2022. [12](#)
- [128] L. Wang, J. Zhang, X. Liu, F. Zhao, Y. Zhang, Y. Zhang, M. Wu, J. Yu, and L. Xu, "Fourier plenotrees for dynamic radiance field rendering in real-time," in *CVPR*, 2022, pp. 13524–13534. [13](#)
- [129] K. Park, U. Sinha, P. Hedman, J. T. Barron, S. Bouaziz, D. B. Goldman, R. Martin-Brualla, and S. M. Seitz, "HyperNeRF: A higher-dimensional representation for topologically varying neural radiance fields," *TOG*, 2021. [13](#)
- [130] W. Xian, J.-B. Huang, J. Kopf, and C. Kim, "Space-time neural irradiance fields for free-viewpoint video," in *CVPR*, 2021. [13](#)
- [131] Z. Li, S. Niklaus, N. Snavely, and O. Wang, "Neural scene flow fields for space-time view synthesis of dynamic scenes," in *CVPR*, 2021, pp. 6498–6508. [13](#)
- [132] E. Tretschk, A. Tewari, V. Golyanik, M. Zollhofer, C. Lassner, and C. Theobalt, "Non-rigid neural radiance fields: Reconstruction and novel view synthesis of a dynamic scene from monocular video," in *ICCV*, 2021, pp. 12959–12970. [13](#)
- [133] Y. Du, Y. Zhang, H.-X. Yu, J. B. Tenenbaum, and J. Wu, "Neural radiance flow for 4d view synthesis and video processing," in *2021 IEEE/CVF International Conference on Computer Vision (ICCV)*. IEEE Computer Society, 2021, pp. 14304–14314. [13](#)
- [134] K. Kania, K. M. Yi, M. Kowalski, T. Trzciński, and A. Tagliasacchi, "CoNeRF: Controllable neural radiance fields," in *CVPR*, 2022, pp. 18623–18632. [13](#)
- [135] J. Sun, X. Wang, Y. Zhang, X. Li, Q. Zhang, Y. Liu, and J. Wang, "FENeRF: Face editing in neural radiance fields," in *CVPR*, 2022. [13](#), [16](#)
- [136] N. Müller, A. Simonelli, L. Porzi, S. R. Bulò, M. Nießner, and P. Kotschieder, "AutoRF: Learning 3d object radiance fields from single view observations," in *CVPR*, 2022, pp. 3971–3980. [13](#), [17](#)
- [137] C. Z. Lin, D. B. Lindell, E. R. Chan, and G. Wetzstein, "3D GAN inversion for controllable portrait image animation," in *ECCV Workshop*, 2022. [13](#), [16](#)
- [138] P. Bojanowski, A. Joulin, D. Lopez-Paz, and A. Szlam, "Optimizing the latent space of generative networks," *arXiv preprint arXiv:1707.05776*, 2017. [13](#), [14](#)
- [139] I. Goodfellow, J. Pouget-Abadie, M. Mirza, B. Xu, D. Warde-Farley, S. Ozair, A. Courville, and Y. Bengio, "Generative adversarial networks," *Communications of the ACM*, 2020. [13](#), [14](#)
- [140] J. Ho, A. Jain, and P. Abbeel, "Denosing diffusion probabilistic models," in *NeurIPS*, vol. 33, 2020, pp. 6840–6851. [13](#)
- [141] J. Song, C. Meng, and S. Ermon, "Denosing diffusion implicit models," in *ICLR*, 2021. [13](#)
- [142] P. Henzler, N. J. Mitra, and T. Ritschel, "Escaping Plato's cave: 3D shape from adversarial rendering," in *ICCV*, 2019. [14](#)
- [143] V. Sitzmann, J. N. Martel, A. W. Bergman, D. B. Lindell, and G. Wetzstein, "Implicit neural representations with periodic activation functions," in *NeurIPS*, 2020. [14](#)
- [144] Y. Xue, Y. Li, K. K. Singh, and Y. J. Lee, "GIRAFFE-HD: A high-resolution 3d-aware generative model," in *CVPR*, 2022. [15](#), [16](#)
- [145] Z. Shi, Y. Xu, Y. Shen, D. Zhao, Q. Chen, and D.-Y. Yeung, "Improving 3d-aware image synthesis with a geometry-aware discriminator," in *NeurIPS*, 2022. [16](#)
- [146] D. Roich, R. Mokady, A. H. Bermano, and D. Cohen-Or, "Pivotal tuning for latent-based editing of real images," *TOG*, 2022. [16](#)
- [147] A. Sauer, K. Schwarz, and A. Geiger, "StyleGAN-XL: Scaling StyleGAN to large diverse datasets," in *SIGGRAPH*, 2022. [17](#)
- [148] R. Mokady, O. Tov, M. Yarom, O. Lang, I. Mosseri, T. Dekel, D. Cohen-Or, and M. Irani, "Self-distilled StyleGAN: Towards generation from internet photos," in *SIGGRAPH*, 2022. [17](#)